ISTANBUL TECHNICAL UNIVERSITY ★ GRADUATE SCHOOL

THE EFFECT OF BILGE KEEL ON THE ROLL MOTION OF A NAVAL DESTROYER

M.Sc. THESIS

Erhan SÖKMEN

Department of Shipbuilding and Ocean Engineering

Shipbuilding and Ocean Engineering Programme

DECEMBER 2024

ISTANBUL TECHNICAL UNIVERSITY ★ GRADUATE SCHOOL

THE EFFECT OF BILGE KEEL ON THE ROLL MOTION OF A NAVAL DESTROYER

M.Sc. THESIS

Erhan SÖKMEN
(508211104)

Department of Shipbuilding and Ocean Engineering

Shipbuilding and Ocean Engineering Programme

Thesis Advisor: Prof. Dr. Kadir SARIÖZ

DECEMBER 2024

<u>İSTANBUL TEKNİK ÜNİVERSİTESİ ★ LİSANSÜSTÜ EĞİTİM ENSTİTÜSÜ</u>

BİR SAVAŞ GEMİSİNİN YALPA HAREKETİ ÜZERİNDE YALPA OMURGASININ ETKİSİ

YÜKSEK LİSANS TEZİ

Erhan SÖKMEN
(508211104)

Gemi ve Deniz Teknolojisi Mühendisliği Anabilim Dalı

Gemi ve Deniz Teknolojisi Mühendisliği Programı

Tez Danışmanı: Prof. Dr. Kadir SARIÖZ

ARALIK 2024

Erhan SÖKMEN, a M.Sc. student of İTU Graduate School student ID 508211104 successfully defended the thesis entitled "THE EFFECT OF BILGE KEEL ON THE ROLL MOTION OF A NAVAL DESTROYER", which he prepared after fulfilling the requirements specified in the associated legislations, before the jury whose signatures are below.

Thesis Advisor :	**Prof. Dr. Kadir SARIÖZ** İstanbul Technical University	....
Jury Members :	**Prof. Dr. Devrim Bülent DANIŞMAN** İstanbul Technical University	....
Jury Members :	**Prof. Dr. Ahmet Dursun ALKAN** Yıldız Technical University	....

Date of Submission : 11 November 2024
Date of Defense : 03 December 2024

To my parents and my beloved spouse...

FOREWORD

I would like to express my deepest gratitude to Prof. Dr. Kadir SARIÖZ for allowing me to work on this thesis with him and for his great support. I also thank my parents, who have always supported me throughout my academic life, including during my master’s program. I would like to extend my heartfelt thanks to my beloved spouse, who never withheld her support during my master’s studies and thesis process.

December 2024

Erhan SÖKMEN
(Mechanical Engineer)

TABLE OF CONTENTS

Pages

FOREWORD ix
TABLE OF CONTENTS xi
ABBREVIATIONS xiii
LIST OF TABLES xvii
LIST OF FIGURES xix
SUMMARY xxi
ÖZET xxiii
1. INTRODUCTION 1
1.1. Literature Review 1
1.2. Thesis Objectives 13
1.3. Contents of The Thesis 14
2. STABILIZATION OF ROLL MOTION 15
2.1. Passive Roll Stabilization 15
2.1.1. Bilge keels 16
2.1.2. Passive anti roll tanks 18
2.2. Active Roll Stabilization 20
2.2.1. Gyroscopes 20
2.2.2. Active anti roll tanks 25
2.2.3. Active fin stabilizers 25
2.2.4. Rudder roll stabilization 27
3. BACKGROUND THEORY OF AQWA© 31
3.1. Hydrodynamic Radiation and Diffraction Analysis by Source Distribution Method 31
3.1.1. Radiation and diffraction wave forces 32
3.1.2. Source distribution method 32
3.2. Dynamics of Floating Bodies 35
3.3. Roll Motion In Regular Waves 37
3.4. Response Amplitude Operators 38
4. ROLL MOTION PREDICTION by AQWA© 41
5. IKEDA METHOD FOR ESTIMATING VISCOUS ROLL DAMPING 45
5.1. Skin Friction Damping 45
5.2. Lift Damping 46
5.3. Eddy Damping and Bilge Keel Damping 47
5.4. Critical Damping Method 48
6. EFFECT OF BILGE KEEL DIMENSIOS ON ROLL MOTION 53
6.1. Validation of Bare Hull DTMB 5415 Hull 53
6.2. Parametric Analyses of DTMB 5415 Hull 56
7. CONCLUSIONS 65
REFERENCES 67
CIRRUCULUM VITAE 73

ABBREVIATIONS

CFD	: Computational Fluid Dynamics
DES	: Detached Eddy Simulation
DoF	: Degree of Freedom
DVM	: Discrete Vortex Method
EFD	: Experimental Fluid Dynamics
FNPF	: Fully Nonlinear Potential Flow Method
FSRVM	: Free Surfac Random Vortex Method
KC	: Keulegian-Carpenter
RAO	: Response Amplitude Operator
RRS	: Rudder Roll Stabilization
PIV	: Particle Image Velocimetry
SSFSRVM	: Slender Ship Free Surface Random Vortex Method
VCG	: Vertical Center of Gravity
VOF	: Volume of Fluid

SYMBOLS

$\mathbf{C_D}$: Drag coefficient
$\mathbf{C_I}$: Inertia coefficient
$\boldsymbol{\omega}$: Frequency
$\boldsymbol{\omega_e}$: Encounter frequency
$\boldsymbol{\rho}$: Density of water
$\mathbf{R_0}$: Roll amplitude
$\mathbf{b_{44}}$: Roll damping coefficient
$\mathbf{c_{44}}$: Restoring coefficient
$\boldsymbol{\phi}$: Roll angle of ship
$\dot{\boldsymbol{\phi}}$: Roll velocity of ship
$\ddot{\boldsymbol{\phi}}$: Roll acceleration of ship
$\mathbf{M_s}$: Stabilizing moment
$\boldsymbol{\Delta}$: Displacement
$\mathbf{T}$: Draft
$\mathbf{A_f}$: Fin area based on wave slope capacity
$\mathbf{C_L}$: Coefficient of lift
$\mathbf{M_r}$: Axis moment
$\mathbf{M}$: Mass matrix
$\mathbf{A}$: Added mass matrix
$\mathbf{B}$: Damping matrix
$\mathbf{C}$: Restoring force matrix
$\mathbf{B_W}$: Wave damping
$\mathbf{B_F}$: Skin friction damping
$\mathbf{B_E}$: Eddy damping
$\mathbf{B_L}$: Lift damping
$\mathbf{B_{BK}}$: Bilge keel damping
$\mathbf{B}_{v}$: Viscous damping
$\mathbf{B}_{cr}$: Critical damping

LIST OF TABLES

Page

Table 2.1 : Comparison of roll damping methods for naval ships **32**
Table 3.1 : Motion, velocity and force/moment components **38**
Table 4.1 : The dimensions of the rectangular and circular cylinders **43**
Table 4.2 : Comparison of Vugt's rectangular section roll damping experiments and AQWA© results **45**
Table 6.1 : Main particulars of US navy destroyer hull 5415 .... **57**
Table 6.2 : Roll non-dimensional values obtained by experiment............... ………**58**
Table 6.3 : Roll non-dimensional values obtained by AQWA© **59**
Table 6.4 : Dimensions of bilge keels.. **60**
Table 6.5 : BK060 bilge keel non-dimensional roll η_{44}/kA values......................... **61**
Table 6.6 : BK160 bilge keel non-dimensional roll η_{44}/kA values......................... ***62***
Table 6.7 : BK260 bilge keel non-dimensional roll η_{44}/kA values............. ………**63**
Table 6.8 : BK030 bilge keel non-dimensional roll η_{44}/kA values......................... **64**
Table 6.9 : BK130 bilge keel non-dimensional roll η_{44}/kA values......................... **65**
Table 6.10 : BK230 bilge keel non-dimensional roll η_{44}/kA values....................... **66**
Table 6.11 : Non-dimensional roll η_{44}/kA values at natural frequencies **67**
Table 6.12 : Non-dimensional roll η_{44}/kA damping (%) at natural frequencies...... **67**

LIST OF FIGURES

Page

Figure 2.1 : Conventional bilge keel arrangement **19**
Figure 2.2 : Bilge keel section for a typical large vessel keel for large vessel **19**
Figure 2.3 : Passive anti-roll tank its geometric parameters. **22**
Figure 2.4 : Angular momentum of rotating flywheel. **23**
Figure 2.5 : Change of angular momentum of the gyroscope.................................. **24**
Figure 2.6 : Creation of stabilizing moment. **24**
Figure 2.7 : Active anti-roll tank.. **26**
Figure 2.8 : Typical active fin stabilizer on a cruise ship. **28**
Figure 2.9 : Fixed fin stabilizer forces. **30**
Figure 2.10 : Rudder roll induced rolling force diagram … **31**
Figure 3.1 : Panel model of DTMB 5415 in AQWA© **36**
Figure 4.1 : The panel model of rectangular shaped floating body **44**
Figure 4.2 : The panel model of cylindrical shaped floating body **44**
Figure 4.3 : Comparison of Vugts' body roll damping of rectangular section **46**
Figure 4.4 : Comparison of Vugts' body roll damping of semi-cylindrical section **46**
Figure 5.1 : Ship-like cross section with bilge **51**
Figure 5.2 : Generic critical damping angular roll motion versus time. **54**
Figure 5.3 : Generic freely-decaying record. **55**
Figure 5.4 : %a of the critical damping angular roll motion versus time. **56**
Figure 6.1 : DTMB 5415 Model **58**
Figure 6.2 : Comparison of experiment and AQWA© non-dimensional roll of DTMB 5415 .... ………**59**
Figure 6.3 : BK060 bilge keel non-dimensional roll $\boldsymbol{\eta_{44}}/kA$ graphics **61**
Figure 6.4 : BK160 bilge keel non-dimensional roll η_{44}/kA graphics..................... **62**
Figure 6.5 : BK260 bilge keel non-dimensional roll η_{44}/kA graphics..................... **63**
Figure 6.6 : BK030 bilge keel non-dimensional roll η_{44}/kA graphics..................... **64**
Figure 6.7 : BK130 bilge keel non-dimensional roll η_{44}/kA graphics. **65**
Figure 6.8 : BK230 bilge keel non-dimensional roll η_{44}/kA graphics. **66**

THE EFFECT OF BILGE KEEL ON THE ROLL MOTION OF A NAVAL DESTROYER

SUMMARY

In this master's thesis, ship roll damping systems have been examined, and the effectiveness of bilge keel as a roll damping system has been parametrically evaluated using the DTMB 5415 high speed displacement hull form.

Roll motions pose a range of problems that can adversely affect the performance of marine vessels. These motions can cause damage to the ship's cargo, decrease crew efficiency, and negatively impact weapon systems on warships. Additionally, roll motions can create issues during aircraft and helicopter landings and takeoffs on warships and reduce the accuracy of weapon systems.

Systems used to control roll motions are generally categorized into two main types: active and passive roll damping systems. These systems aim to reduce roll motions through various methods. The roll damping measures discussed are as follows:

Passive roll damping systems include bilge keels and passive roll reduction tanks. Bilge keels are a traditional, cost-effective method that effectively dampens roll motions. They are simple to manufacture and are often combined with active systems on warships. Passive roll reduction tanks, on the other hand, achieve roll damping by balancing the movement of liquids within the vessel.

Active roll damping systems feature gyro stabilizers, active roll reduction tanks, fin stabilizers, and rudder-controlled stabilizers. Gyro stabilizers are highly effective at low speeds and during anchorage, as they operate within a fully enclosed box, protecting them from external damage. This design allows for safe navigation in shallow waters. Active roll reduction tanks actively balance the ship's motion, while fin stabilizers mitigate rolling caused by waves or external forces.

These stabilizers use sensors and control systems to dynamically adjust their fins, ensuring effective roll damping. Fin stabilizers must remain submerged during ship inclination, be located in protected areas of the hull, and minimize water flow disturbance.

To address collision risks, foldable fins have been developed, allowing retraction when not in use. Despite their high cost, fin stabilizers are highly efficient, particularly in challenging sea conditions, and are widely used on various vessels, including yachts, cruise ships, warships, and cargo ships.

Additionally, they must be installed in a manner that does not disturb the water flow. Active fin stabilizer systems, being mounted on the exterior of the ship, pose a collision risk; thus, foldable fins have been developed.

These foldable fins can be retracted into the vessel when not in use, thereby minimizing additional resistance to the ship. Fin stabilizers are particularly effective in challenging conditions such as head seas and cross seas and are considered the most efficient equipment for roll damping. Advanced fin stabilizers are now produced for a wide range of vessels, from yachts and cruise ships to warships and commercial cargo ships. Despite their high cost, these systems are preferred for their effective performance.

Rudder roll stabilizers use the ship's rudder to balance roll motions. However, they are generally not effective at low speeds and while the ship is at anchor. Rudder-controlled roll stabilization systems are advantageous because they do not add extra weight or volume to the ship.

The history of roll damping systems began with William Froude's free surface tanks and Frahm's U-type passive roll tanks. The use of bilge keels extends back to the early 20th century, with fin systems beginning to be employed in the 1930s.

In the subsequent sections of the study, parametric analyses have been conducted using different bilge keel geometries on the 5415 model bare hull to investigate the effect of bilge keels on roll damping. Prior to these parametric analyses, a validation was performed by comparing experimental roll damping results of the 5415 model bare hull with results from AQWA© software. This comparison yielded highly favorable results.

Ikeda's viscous roll damping method has been thoroughly examined to account for viscous effects in validation and parametric analyses. The Ikeda method has been used to detail and examine the critical roll damping method and calculation techniques. When viscous effects are incorporated into the AQWA© program, the roll values for the structure are found to be very close to the expected values by experiments.

Following the completion of the validation work, parametric analyses were performed using AQWA© software with a total of six different bilge keels, utilizing the bilge keels of the DTMB 5415 model ship. In these parametric analyses, the angle, width, and length of the bilge keels were systematically varied, and the model ship was analyzed with these bilge keels at different speeds. The analyses concluded that examining parameters such as the width, length, and angle of the bilge keels individually would be insufficient; instead, all relevant parameters should be considered together in the analysis.

BİR SAVAŞ GEMİSİNİN YALPA HAREKETİ ÜZERİNDE YALPA OMURGASININ ETKİSİ

ÖZET

Bu yüksek lisans tez çalışmasında gemi yalpa hareketlerini sönümleyen sistemler incelenmiş ve DTMB 5415 destroyer formu ele alınarak bir yalpa sönümlendirme sistemi olarak yalpa omurgasının yalpa hareketindeki etkinliği parametrik olarak incelenmiştir.

Yalpa hareketi, geminin stabilize olmasını zorlaştıran, hem operasyonel hem de güvenlik açısından ciddi riskler taşıyan bir hareket türüdür. Geminin yalpa yapması, yük dengesi üzerinde olumsuz etkiler yaratabilir ve bu da gemi yükünün zarar görmesine yol açabilir. Yalpa hareketleri aynı zamanda gemi personelinin çalışma verimliliğini düşürebilir ve gemi içindeki ekipmanların hasar görmesine neden olabilir.

Yalpa sönümleme sistemlerinin gelişimi, denizcilik sektöründe önemli bir ilerleme kaydetmiştir. İlk yalpa sönümleme sistemlerinden biri, serbest yüzey tanklarıyla William Froude tarafından geliştirilmiştir. Froude, serbest yüzey tankları kullanarak gemi yalpa hareketlerini kontrol altına almayı başarmış ve bu alandaki ilk önemli adımlardan birini atmıştır. Daha sonraki yıllarda, U tipinde pasif yalpa tankları Frahm tarafından tanıtılmıştır. Frahm'ın bu yenilikçi tasarımı, yalpa sönümleme sistemlerinin gelişimine önemli bir katkı sağlamış ve denizcilik sektöründe büyük yankı uyandırmıştır.

Yalpa omurgalarının kullanımı ise 20. yüzyılın başlarına kadar uzanmaktadır. Yalpa omurgaları, gemi stabilizasyonunu sağlamak için basit ve etkili bir yöntem olarak kabul edilmiştir. Fin stabilizerlerin kullanımı ise 1930'lu yıllarda başlamış ve bu sistemler zamanla denizcilik endüstrisinde yaygın olarak kullanılmaya başlanmıştır. Fin stabilizerlerin avantajları, bu sistemlerin gelişimini hızlandırmış ve günümüzde birçok farklı tipte deniz aracı için tercih edilen bir stabilizasyon sistemi haline gelmiştir.

Savaş gemileri gibi özel amaçlı deniz araçlarında, yalpa hareketlerinin etkisi çok daha kritik olabilir. Yalpa hareketi, savaş gemilerinde yer alan silah sistemlerinin isabet oranını olumsuz etkileyebilir ve geminin operasyonel verimliliğini azaltabilir. Bu durumda, geminin görev kabiliyeti önemli ölçüde azalabilir. Özellikle savaş operasyonlarında, yalpa hareketlerinin kontrol edilememesi, geminin stratejik avantajını kaybetmesine neden olabilir. Ayrıca savaş gemilerindeki helikopter ve uçakların iniş-kalkış operasyonları da bu hareketlerden olumsuz etkilenebilir. Yalpa hareketinin kontrol altına alınması, hem operasyonel verimliliği artırmak hem de gemi içi ekipmanların ve personelin güvenliğini sağlamak açısından önemlidir. Bu sistemler, aktif ve pasif yalpa sönümleme sistemleri olarak iki ana kategoriye ayrılmaktadır. Aktif ve pasif sistemler, farklı çalışma prensiplerine sahip olsalar da,

her ikisinin de amacı gemi yalpa hareketlerini minimum seviyeye indirmektir. Pasif sistemler, genellikle dışarıdan bir müdahale gerektirmeden, geminin yapısal özellikleri veya iç mekanizmaları kullanılarak yalpa hareketlerini azaltmayı amaçlar. Aktif sistemler ise, geminin yalpa hareketlerine anında müdahale ederek bu hareketleri kontrol altına almayı hedefler. Tez çalışmasında bu sistemlerin işleyişi detaylı bir şekilde ele alınmıştur.

Pasif yalpa sönümleme sistemleri, geminin yalpa hareketlerini herhangi bir dış müdahale olmadan, yapısal veya mekanik unsurlar kullanarak sönümlemeye çalışır. Bu sistemlerin en bilinen örneklerinden biri, yalpa omurgalarıdır. Yalpa omurgaları, geminin iki yanına yerleştirilen ve yalpa hareketini azaltmaya yarayan sabit yüzeylerdir. Bu omurgalar, gemi gövdesine eklenerek yalpa hareketlerini kontrol altına alır. Yalpa omurgaları imalat açısından avantajlıdır. Özellikle maliyet etkin bir çözüm sunarlar ve bu nedenle sıkça tercih edilirler. Yalpa omurgalarının bir diğer önemli avantajı ise, pasif bir sistem olmalarına rağmen, farklı hızlarda etkin performans gösterebilmeleridir. Bu özellikleri sayesinde, savaş gemilerinde aktif stabilizasyon sistemleriyle birlikte kullanılarak, geminin yalpa hareketlerini minimuma indirmeye yardımcı olurlar.

Pasif sistemler arasında yer alan bir diğer önemli çözüm ise pasif yalpa önleyici tanklardır. Bu sistemler, geminin içine yerleştirilen tanklar aracılığıyla yalpa hareketlerini dengelemeyi amaçlar. Tankların içine doldurulan sıvı, gemi yalpa yaptığında karşı tarafa doğru hareket eder ve bu hareket, geminin yalpa dengesini sağlamada yardımcı olur. Pasif yalpa önleyici tanklar, özellikle büyük deniz araçlarında sıkça kullanılır ve geminin genel stabilitesini artırmada etkili bir rol oynarlar. Bu sistemler, herhangi bir aktif müdahale gerektirmeden, gemi hareketlerine otomatik olarak yanıt verir ve bu sayede yalpa hareketlerini sönümlemede etkin bir rol oynar.

Aktif yalpa sönümleme sistemleri ise, geminin yalpa hareketlerini aktif bir şekilde kontrol altına almayı hedefleyen daha gelişmiş sistemlerdir. Bu sistemler, genellikle elektronik veya mekanik bileşenler yardımıyla gemi hareketlerine anında müdahale ederler ve yalpa hareketlerini minimuma indirirler. Aktif sistemler arasında en bilinenlerinden biri, cayro stabilizerlerdir. Cayro stabilizerler, özellikle düşük hızlarda veya gemi demirlediğinde dahi yalpa hareketlerini etkin bir şekilde kontrol altında tutabilirler. Bu sistemler, tamamen kapalı bir sistem olarak çalışır ve dışarıdan gelebilecek hasarlardan korunurlar. Cayro stabilizerlerin bu kapalı sistem yapısı, geminin dış etkenlerden etkilenmeden stabilizasyon sağlayabilmesine olanak tanır. Özellikle lüks yatlar ve askeri gemilerde cayro stabilizerlerin tercih edilmesinin sebeplerinden biri, bu sistemlerin sığ sularda da etkin performans gösterebilmesidir.

Bir diğer aktif sönümleme sistemi, aktif yalpa önleyici tanklardır. Bu sistemler, pasif tankların aksine, aktif bir müdahale mekanizması ile çalışır ve gemi hareketlerini aktif olarak dengelemeye çalışırlar. Gemi yalpa yaptığında, tank içindeki sıvıların hareketi aktif olarak kontrol edilir ve bu hareket, geminin yalpa dengesini sağlar. Bu sistemler, özellikle büyük deniz araçlarında tercih edilir ve açık deniz koşullarında etkin performans gösterirler.Fin stabilizerler ise, aktif yalpa sönümleme sistemleri arasında en yaygın olarak kullanılan sistemlerden biridir. Bu sistemler, geminin gövdesine monte edilen kanatlar aracılığıyla çalışır. Fin stabilizerlerin en büyük avantajı, geminin hareketlerini dengeleme için suyla etkileşime giren yüzeysel kanatlar kullanmalarıdır.

Bu sayede, gemi yalpa hareketi yaptığında, fin stabilizerler devreye girerek bu hareketi dengelerler. Fin stabilizerlerin etkinliği, geminin hızına ve dalga koşullarına bağlı olarak değişiklik gösterebilir. Ancak bu sistemler, zorlu deniz koşullarında dahi etkili bir stabilizasyon sağlayabilirler.

Fin stabilizerlerin bir diğer önemli avantajı, katlanabilir versiyonlarının da mevcut olmasıdır. Bu sistemler, kullanılmadıkları zaman gemi içine katlanarak çekilebilir ve bu sayede gemi dışına ek direnç oluşturmazlar. Katlanabilir fin stabilizerler, özellikle dar alanlarda veya sığ sularda seyir yaparken büyük avantaj sağlarlar. Günümüzde fin stabilizerler, yat endüstrisinden ticari gemilere kadar birçok farklı tipte deniz aracı için tercih edilen bir stabilizasyon sistemi haline gelmiştir. Bu sistemler yüksek maliyetli olmasına rağmen, sundukları etkin performans sayesinde tercih edilmektedirler.

Dümen kontrollü stabilizerler, aktif yalpa sönümleme sistemleri arasında yer alan bir diğer önemli sistemdir. Bu sistemler, geminin dümenini kullanarak yalpa hareketlerini kontrol etmeyi amaçlar. Dümen kontrollü sistemler, genellikle düşük hızlarda etkili olsalar da, demirleme sırasında yeterli performansı sağlayamayabilirler. Bununla birlikte, bu sistemlerin en büyük avantajı, gemi içinde ek hacim kaplamamaları ve fazladan donanım ağırlığı oluşturmamalarıdır. Bu özellikleri sayesinde, dümen kontrollü sistemler gemi tasarımında esneklik sağlar ve gemi içindeki yerleşim alanının daha verimli kullanılmasına olanak tanır.

Bu tez çalışmasında, ilerleyen bölümlerde validasyon analizi ve parametrik analizleri gerçekleştirebilmek maksadıyla viskoz etkilerin analizlerde hesaba katılabilmesi için Ikeda’nın viskoz yalpa sönümleme metodu kritik sönümleme metodu ile birlikte detaylı olarak incelenmiştir. Ikeda metodu kullanılarak kritik yalpa sönümleme metodu ve hesaplama yöntemleri detaylı bir şekilde açıklanmıştır. Bahse konu viskoz etkiler AQWA© programına tanımlandığında, yapıya ait yalpa değerleri olması gereken değerlere oldukça yakın seyretmektedir.

Çalışmanın müteakip bölümlerinde, yalpa omurgasının yalpa sönümleme üzerine etkisini incelemek maksadıyla farklı yalpa omurga geometrileri kullanılarak DTMB 5415 model çıplak tekne üzerinde parametrik analizler yapılmıştır. Parametrik analizlere başlanmadan önce 3-B panel yöntemi tabanlı AQWA© yazılımının doğrulanması amacıyla DTMB 5415 model çıplak tekne deneysel yalpa sönümleme sonuçları, AQWA© ‘da analizi yapılan DTMB 5415 çıplak tekne modeli sonuçlarıyla karşılaştırılmış ve son derece olumlu sonuçlar elde edilmiştir.

Doğrulama çalışmasının tamamlanmasına müteakip DTMB 5415 model gemisinin sahip olduğu yalpa omurgasından faydalanılarak toplamda 6 farklı yalpa omurgası ile AQWA© yazılımı kullanılarak parametrik analizler yapılmıştır. Bahse konu parametrik analizlerde yalpa omurgalarının açısı, genişliği ve uzunluğu sistematik olarak değiştirilmiş ve model gemi bahse konu yalpa omurgaları ile farklı hızlarda analize tabi tutulmuştur. Yapılan analizler yalpa omurgasının genişlik, uzunluk, açı gibi parametrelerinin bireysel olarak incelenmesinin eksik bir çalışma olacağı, yapılan çalışmalarda bahse konu tüm parametrelerin hesaba katılarak analiz yapılması gerektiği sonucuna varılmıştır.

1. INTRODUCTION

Excessive roll motion on vessels gives rise to a range of issues and concerns for ships and maritime operations. Safety risks are prominent, as excessive rolling can lead to accidents and injuries, impacting both passengers and crew. The discomfort caused by motion sickness is another prevalent problem, affecting the well-being of those on board. Structurally, vessels are exposed to stress and potential damage due to prolonged rolling, affecting both the hull and onboard equipment. Cargo vessels face challenges with cargo stability, while operational efficiency can be hindered by difficulties in tasks like loading and maintenance. Excessive roll motion can lead to higher fuel consumption, diminished passenger comfort, and increased crew fatigue. Roll characteristics are key for operational performance, particularly in tasks such as launching and recovering equipment, conducting helicopter operations. Addressing these issues requires a combination of design, technology, and operational measures to ensure safe and efficient maritime operations. On reduction of roll motion bilge keels play an important role, offering significant benefits for comfort, stability, and safety at sea. These longitudinal appendages along the sides of a ship's hull are designed to interact with the water during rolling, generating hydrodynamic forces that effectively counteract and reduce the amplitude of the rolling motion. By reducing roll motion, bilge keels play a role in ensuring structural integrity and safety by reducing the loads induced by rolling forces.

1.1. Literature Review

The early steamships faced challenges achieving high speeds in head seas. However, the lack of aerodynamic damping due to the sails increased the importance of the rolling motion. This could be why Froude [1] initially studied rolling motions. In his study, the ship assumed to sail broadside to the waves, treated as small rafts or corks following the wave slope and orbital motion of wave particles. Froude realised that this assumption is valid only for waves much longer than the ship's width, or at very low motion frequencies. He emphasized the wave slope's impact on ship rolling, stressing the need to extend the natural rolling period rather than shorten it.

Keulegan and Carpenter [2] conducted a study on fluid motion around cylinders and plates by utilizing standing waves in a rectangular basin. The features of the surrounding fluid motion were identified using the relevant standing wave equations and the measured amplitude of the waves. Keulegan and Carpenter determined drag and inertia coefficients and established correlations with the period parameter VT/d. This parameter is commonly used today to assess whether vortex shedding from the bilge is taking place. It considers factors such as the relative flow velocity at the bilge and the roll natural frequency of the vessel.

In his research, Vugts [3] examined the hydrodynamic coefficients of two-dimensional cylinders with various cross-sections. These coefficients were determined through forced oscillation tests and theoretical computations potential theory. The primary aim of the study was to observe heaving, rolling, and swaying motions and to understand the influence of the section shape on these motions. Vugts noted that viscous effects were negligible in heave motion, and sway motion exhibited good agreement with experimental results. However, for roll motion, the results were less promising compared to heave and sway motions. Thus, with this study Vugts was the first to calculate the hydrodynamic coefficients for sharply edged sections in roll motions and observe the importance of the viscous effects.

Ikeda [4] modified the Morison equation to predict roll damping. The equation was linearized, and the inertia component was disregarded under the assumption that it has no impact on roll damping. The study demonstrated that the C_D (drag coefficient) and C_I (inertia coefficient) values are significantly influenced by the KC number. In the context of bilge keels, this non-dimensional number is contingent on the bilge keel height and motion amplitude, remaining independent of the frequency.

Brown [5] formulated a theory for vortex shedding from marine vehicles using the Discrete Vortex Method (DVM). His study primarily emphasizes the correctness of the DVM in depicting the vortex shedding component and its effective prediction when integrated with potential flow theory. The study compares potential flow theory with experimental data, assesses the influence of vortex shedding, but does not directly compare the DVM results with experimental findings. Moreover, the study concludes that the roll center determined from potential flow theory is satisfactory for application in vortex shedding scenarios.

Sarpkaya and O'Keefe [6] performed experiments based on a flat plate attached to a wall in an oscillating flow. Three vortex shedding regimes depending on the Keulegan Carpenter number were identified:

1. KC < 3

2. 3 < KC < 8

3. KC > 8

For KC values less than 3, when a new vortex is formed, it combines with the vortex generated in the preceding motion cycle, resulting in a counter-rotating pair that moves away at a 45-degree upward angle to the left or right of the tip of plate. In the range of 3 to 8, the vortices from previous cycles begin to decay and start orbiting around the newly shed, stronger vortices. When KC exceeds 8, vortex shedding tends towards a stable state where one large vortex is shed in each half cycle, accompanied by various smaller vortices if the longer duration of a cycle permits their development. An increase in the KC number leads to the shedding of more vortices.

Chakrabarti's [7] study on Ikeda's roll damping method identified multiple components contributing to roll damping. For practical total damping calculations, five distinct components are defined. Wave damping, determined through linear diffraction/radiation theory, was found to have a minimal impact on overall roll damping for conventional ship-shaped or barge-like structures. Calculating other roll damping contributions is challenging, leading to empirical expressions for friction, lift, and eddy making damping. Bilge keel presence introduces additional damping, with nonlinear effects linked to roll amplitude. Chakrabarti's formulations consider vessel speed and current.

Taylan [8] conducted a study on the impact of forward speed on the peak roll responses of ships. The study evaluated the stability of ships by considering the effect of several stability parameters. The study found that linear and nonlinear roll damping coefficients change with increasing speed. The study also found that for relatively lower speeds (0-6 knots), the periodic resonance roll peak amplitudes decrease drastically, which improves the ship's roll motion stability. However, the rate of decrease slows down and reaches a specific value at which amplitudes are no longer affected by changing speed. Around 10 knots, the responses are not changing. Taylan stated that the risk of capsizing is much higher when the ship is slowly moving or not moving at all, as far as the roll damping is concerned. He also stated that the effect of speed becomes more evident for Froude numbers greater than 0.22.

Zaraphonitis and Papanikolaou [9] investigated the applicability of a 3D numerical panel method for evaluating the seakeeping performance and structural loads of advanced high-speed vessels. He found that without viscous effects, the panel method’s radiation damping (Ikeda’s wave-making component) is not sufficient by itself. To account for the viscous flow effects on the ship’s behavior at forward speed, he applied a semi-empirical approach to the panel method in his study. He also took into account the other Ikeda's damping components. He discovered that the panel method and experimental results in motions showed good agreement if semi empirical formulas applied.

Ikeda [10] conducted both experimental and theoretical research on heavy parametric rolling in beam waves for passenger ships. In his study, he demonstrated the effect of bilge keels in reducing roll motion. The results of his study indicate that parametric rolling in beam waves can be significant for a large passenger ship if her bilge keels are removed. However, if the ship is equipped with well designed bilge keels, the parametric rolling in beam waves disappears, but that in longitudinal waves does not. Furthermore, as the bilge keel size increases, the critical wave height of parametric rolling in beam waves and its magnitude also increase.

Bassler [11] predicted bilge keel roll damping for a cargo ship, Series 60 and the ONR-T hull form. Comparisons were made for all three ships to highlight differences in bilge keel roll damping for modern hull-form geometries and identifty the limits for application. It has been demonstrated that the damping effect from the interaction between the bilge keel and the hull is constrained by both the size of the bilge keel and the amplitude of the roll motion.

Graham [12] conducted a study on Lagrangian vortex methods to simulate vortex shedding at the bilges and sharp edges of floating structures under the oscillatory flow conditions caused by incident waves and the body's motion in response. The flow around the bilge of a typical long floating hull in beam waves was analyzed on a sectional basis. The isolated edge results were then matched to the outer three-dimensional wave potential flow provided by a standard surface panel method, with the intention of reducing computation time. The study revealed that, compared to a rectangular section, a rounded bilge experiences reduced strength in vortex shedding due to viscous effects, consequently leading to a decrease in the vortex-induced damping force.

Jaouen et al. [13] conducted numerical sensitivity studies to compute the viscous-damping coefficient for various roll amplitudes and periods of rectangular ship forms using URANS code. The results were compared to experimental values, showing good agreement. The influence of grid resolution, time step, and iterative convergence on the viscous damping coefficient was discussed, highlighting the importance of fine grids and an iterative convergence level of 10^{-4}. For a rectangular hull with sharp bilges, comparisons with potential flow code DIFFRAC for free-surface damping and ReFRESCO for other components align well with experimental values, confirming the linear relationship between viscous damping coefficient and roll amplitude for the case. Similar assessments for a hull with triangular-shaped bilge keels show reasonable agreement for dimensionless frequencies below 0.7 but reveal overestimations at higher frequencies.

Miyake [14] investigated bilge keels for a new non-ballast ship featuring a more rounded cross-section. The commercial code Fluent was employed to compute the behavior of a vertical plate mounted on a wall, as well as two vertical plates arranged in tandem on a wall. A CFD study was conducted to visually represent the occurring effects. Experimental findings indicated that the impact of bilge keels on such a rounded ship is considerably smaller compared to conventional ships with square cross-sections, and it significantly relies on the specific locations where the bilge keels are attached. The study demonstrated that two bilge keels positioned closely to each other exert substantial effects on one another.

Irkal et al. [15] studied the effectiveness of bilge keel in improvement of roll damping by conducting experiments on typical Panamax ship model section. The experimental output was used to validate the commercial CFD code. Attachment of bilge keel to the hull section of the ship model improved the roll damping to a significant value and this was very closely replicated in the CFD simulations. The roll response at resonance was reduced to half when compared with the model having no bilge keel. The measured roll RAO compared with that from the CFD simulation show a very good agreement.

A two-dimensional model was designed by Deng et al. [16] to study the impact of bilge keels on damping moments, focusing on forced rolling motion. The model neglects factors like surface wave influence, cylinder-wave interaction, and bilge keel length. Using a viscous code based on the SST k - ω model, the simulation results were verified and validated. Notably, a phase difference between damping moments induced by the cylinder and bilge keels was observed. Total damping is reduced when the bilge keel width reaches a specific size. Increasing the bilge keel width beyond this size minimally affects the cylinder-induced damping moment, but significantly enhances the bilge keel-induced damping, making it the dominant factor in total damping.

URANS simulations investigated viscous bilge keel roll damping in fully submerged bodies with a circular cylinder hull model by Council et al. [17]. Bilge keels ranging from 0.2 to 1.0 m span were tested for roll amplitudes of 2° to 20°, with a 10.6 s period. Hydrodynamic coefficients, obtained through quadratic damping assumption and nonlinear regression, were compared to empirical and flat plate theory values. Generally, as angular amplitude or bilge keel span increased, added mass and damping increased, while drag coefficient decreased. Damping effectiveness depended on the interaction of bilge keel-generated vortices with the rotating body, with hull-bound vortices yielding higher damping. Complex vortex interactions resulted in noisier moment histories.

Falzarano et al. [18] conducted a thorough literature review on diverse approaches to predicting roll damping. In his research, he juxtaposed potential theory programs with empirical formulas to assess their efficacy in calculating roll damping. Notably, he examined the wave-making component calculation using the Ikeda and potential theory programs, presenting the superior performance of potential theory in modeling the wave-making aspect of Ikeda's method. In his study, he asserted that the lift component significantly influences damping as a ship has forward speed. Secondly, he emphasized that the impact of the eddy damping component decreases as the ship maintains a constant forward speed. Moreover, Falzarano highlighted the importance of the beam-to-draft ratio, attributing its significance to the limitations of empirical methods. These methods typically rely on typical cargo ship beam-to-draft ratios (B/T ratios) making the beam-to-draft ratio a key factor in roll damping predictions. Mainly, Falzarano underscored the influence of these hull form characteristics on roll damping, emphasizing the relationship between bilge radius, beam-to-draft ratio, and the accuracy of empirical methods in predicting damping effects.

Gu et al. [19] conducted a study on the roll damping of a two-dimensional FPSO model induced by bilge keels, employing the CFD method. The simulation utilized Star-CCM+, employing the Volume of Fluid (VOF) approach to capture the free surface, and the findings were verified through experimental comparisons. Through multiple simulations, the roll damping coefficient resulting from varying positions of the bilge keels was calculated. The key finding was that bilge keels exhibit higher damping coefficients when placed at the bilge compared to other positions, indicating a more significant impact on roll motion. The positioning of bilge keels on the ship's side and bottom also affects damping, with closer proximity to the bilge resulting in greater damping effectiveness. A comparison between side and bottom locations revealed that bilge keels on the side have a more pronounced influence on roll damping.

Haver [20] conducted a comprehensive study aimed at enhancing the prediction of roll motions in vessels, including sheerlegs and barges, by developing a mathematical model to describe viscous roll damping. The validity of this model was assessed through comparison with available data.

The Vertical Center of Gravity (VCG) has been identified as a significant factor influencing the potential roll damping coefficient. An increase in VCG results in a decrease in this coefficient due to a phase difference between the coupling terms and the roll and sway terms. Interestingly, the VCG also positively affects the viscous roll damping coefficient. It is suggested that the coupled roll-sway motion allows the eddy to remain close to the vessel for an extended period, thereby enhancing the damping effect. Haver developed two models based on the theoretical frameworks established by Ikeda, Tanaka, and Himeno, which effectively determine viscous roll damping for both ship-shaped and barge-type vessels, as long as the geometry and motion conditions meet the boundary conditions of the underlying theory. Additionally, a notable observation highlighted the increasing relevance of potential damping compared to viscous damping contributions as the Breadth-to-Draft (B/T) ratios rise, indicating that potential damping becomes more significant under these conditions.

Park et al. [21] conducted experiments and numerical simulations to estimate the added resistance of a large tanker in oblique waves. The self-propulsion test was employed for seven wave directions ranging from 0 to 180 degrees. The added resistance was determined by the difference between the propeller thrust in calm water and in waves. Experiments were carried out in the SSPA seakeeping basin and were compared with two numerical simulations: the strip method and the 3D Rankine panel method. The results calculated by the Rankine panel method showed good agreement with the experimental findings. Notably, viscous roll damping was considered in the calculations by taking 3% of the critical roll damping (the 3% is obtained through fitting with free roll decay test of the SSPA experiment).

Yıldız et al. [22] conducted a study employing a URANS code to predict the roll damping coefficient across various combinations of roll amplitudes and periods. The investigation focused on the unsteady flow around a 2D midsection subjected to forced rolling with bilge keels. The research involved extensive numerical sensitivity analyses to compute viscous-damping coefficients under diverse conditions. The numerical results were then compared with both experimental values and Ikeda's estimation method. The study revealed that URANS proved capable of accurately predicting the roll damping coefficient. Particularly, the calculations were extended to shallow draft conditions where Ikeda's method is known to be insufficient. It has seen that URANS method comply with experimental results in shallow water study.

The problem of predicting the roll damping coefficient of an FPSO with bilge keel was studied numerically and experimentally by Ommani et al. [23]. The aim was to identify how the roll damping coefficient is changing with the bilge keel height. Two-dimensional numerical simulations for forced roll motion of the FPSO's mid-section were carried out using the hybrid code PVC-2DRoll. The estimated roll natural period was chosen as the forcing frequency. The rotation center and bilge keel was varied in order to study the dependency of the damping coefficients to these factors. It was shown that moving the center of rotation up and further away from the water line, increases the non-linear part of the roll damping while decreasing the linear part. The slope reduction of the roll damping as a function of the roll amplitude was addressed and attributed to the free surface effects. Potential flow calculations were performed using WAMIT to obtain the roll critical damping, as well as linear wave radiation damping. Furthermore, it was shown that the roll damping due to wave radiation decreases by increasing the bilge keel height for the shape studied.

Experimental and CFD simulations were conducted on a typical Panamax ship model, exploring six bilge keel dimensions at three draft levels by Irkal [24]. CFD accurately reproduced measured free roll decay time histories for various heel angles, showing good agreement. Radiated wave surface elevations from experiments matched simulation results. Comparison of PIV experiments and CFD revealed similar vortex shedding patterns contributing to roll damping. Adding a bilge keel significantly increased hull roll damping, with wider keels leading to greater effects. Horizontal bilge keels provided damping comparable to inclined ones (45 degrees), while vertical keels induced less damping. Without a bilge keel, roll damping was linear; with a keel, nonlinearity increased with width. Extensive comparisons confirmed the practical utility of CFD in estimating roll damping and predicting roll motion.

Jiang [25] has proposed and successfully implemented the SSFSRVM (Slender Ship Free Surface Random Vortex Method) model to simulate the free roll decay motion of a INSEAN C2340 hull model. The SSFSRVM model is capable of predicting the roll motion of a hull and simulating the dominant behavior of the longitudinal vortical structures in the fluid, in comparison with documented PIV images. The SSFSRVM model was claimed to be computationally more efficient than mesh-based CFD methods and yet can capture significant flow details. He also stated in his study that the effect of bilge keel span on the roll decay coefficient is non-proportional to the rate of increase of the bilge keel span. A bilge keel longer span generates stronger counter-rotating vorticity pairs, which transfers more energy from the hull into the surrounding flow and leads to a larger decay rate. In the cases of roll motion in waves, increasing the bilge keel span decreases the roll amplitude up to %32.

Gökçe and Kınacı [26] numerically solved the free roll decay of the benchmark DTMB 5415 hull with bilge keels in calm water by applying computational fluid Dynamics (CFD). He investigated the contributions of viscosity, wave, eddy, and forward ship speed separately for ship roll damping, which were integral parts of the experimental setups. The numerical results were first validated with free roll decay experiments. Additionally, mathematical derivations of ship roll response were used where experiments were impractical or inapplicable. Gökçe made a detailed analysis for the numerical estimation of roll damping on DTMB 5415 hull. The study shows the model captured the decay trend but inaccurately estimated the ship's natural rolling frequency.

A validated 2D-CFD simulation approach was employed for prescribed sinusoidal roll motion of a generic vessel model by Irkal et al. [27], using experimental data. The simulated roll added mass and damping coeffcients closely matched the experimental results. The simulations focused on rounded bilge ship mid-sections, investigating roll motion across seven frequencies. The rounded bilge model, both with and without a bilge keel, underwent oscillations, revealing that the bilge keel attachment enhanced roll damping by 60-80% across all tested frequencies. The roll added mass of the model increased by 90% with the bilge keel attachment across all frequency ranges, with a slight rise associated with roll amplitude. The rise in roll damping was particularly notable with increasing roll frequency and amplitude, indicating a pronounced effect at higher frequencies due to intensified vortex formation and shedding. He derived vorticity plots from the 2D-CFD simulations offered offering insights into the flow dynamics around the hull.

The flow around a two-dimensional conventional ship cross-section with a forced rolling motion under the influence of free surface was investigated by Yıldız and Yılmaz [28] using a RANS solver, and the roll damping coefficients were calculated. The results were observed to be in good agreement with experiments, demonstrating the applicability of numerical solvers in roll damping calculations. Numerical analyses were conducted for different bilge keel widths within the scope of this study. Damping originating from the bilge keel constitutes significant portion of the total roll damping. The most important factor contributing to this damping is the vortices generated by the bilge keel. Numerical analyses were performed for three different bilge keel widths, and it was observed that a wider bilge keel increases roll damping. Vortices around the bilge keel for three different keel widths were presented, showing that the size of the vortices increases with the widening of the bilge keel. This increase has led to an enhancement in viscous roll damping originating from the bilge keel. The obtained results indicate that the numerical method is a viable alternative for calculating roll damping and can be utilized in the future development of new methodologies.

Irkal et al. [29] studied roll motion of a barge-like ship model both with and without bilge keel, including experimental validation. and added mass with experimental data reveals good agreement. The application of large eddy simulation to this type problem is explored and discussed. It is noted that Ikeda's semi-empirical method tends to over-predict roll damping at larger roll angles. The pressure distribution aft of the bilge keel is found to deviate, while the pressure in front of the bilge keel closely aligns with semi-empirical calculations. The study concludes that the effects of bilge keel thickness, degrees of freedom, and scaling on roll motion and damping are insignificant for the selected barge-like ship model.

Kim et al. [30] conducted a study to investigate the interaction between the roll and heave motions, especially the heave influence on the roll motion of the 2-D rectangular structure in beam sea conditions. It is was concluded that the heave motion has a significant impact on the viscous effects as well as the roll motion, and that the roll motion has the nonlinear characteristics with the wave steepness. He revealed that the heave influence on the roll motion has to be considered to estimate accurate roll motion of floating structures.

Lungu [31] conducted numerical simulations focusing on the free roll decay of a double-symmetric floating cylindrical hull equipped with bilge keels. His study, employing an unsteady viscous flow solver, emphasized the significant impact of viscous effects on the roll motions experienced by floating bodies. Lungu proposed a DES-based (Detached Eddy Simulation) approach for predicting roll damping and motion of ships, acknowledging its computational demands. Lungu's findings indicate that during the damping process, the intensity of eddies decreases as the roll angle diminishes. Moreover, an escalation in the initial roll angle results in an increased eddy intensity, leading to a higher expenditure of turbulent kinetic energy for stabilizing the hull motion. Notably, the damping coefficient calculated for a hull equipped with two bilge keels is greater for average roll angles exceeding 40 degrees. This implies that the efficiency of bilge keels becomes more prominent than viscous effects in influencing the damping process at higher average roll angles.

Ibinabo and Tamunodukobipi [32] seeked to present a detailed method of computing the Response Amplitude Operator(s) (RAOs) for the six (6) degrees of freedom using ANSYS AQWA. The analysis is performed with frequency and directional discretization. The motion and resistance coefficients are determined in six (6) degrees of freedom and for a range of wave frequencies and wave directions. This information is stored in a ship characteristics data base that is subsequently applied for the time domain analysis. He calculated roll RAO values succesfully.

By Asis et al., [33] the roll motion of a traditional wooden boat with and without bilge keel was analyzed. According to the study, the bilge keel position with a slope of 15 degrees induced the most significant effect on increasing the linear and the nonlinear damping coefficients compared to the bilge keels position with a slope of 30 degrees and 45 degrees.

A Panamax ship model's two-dimensional roll decay is simulated using the free surface random vortex method (FSRVM) by Jieng et al. [34] . Additional roll damping from bilge keels of varying heights and installation angles is compared. The effects of bilge-keel configurations on roll motion under regular waves are discussed, revealing characteristics and mechanisms affecting roll damping reduction. Comparisons with experiments verify the feasibility of the modified FSRVM. Critical conclusions include the discovery that bilge keels cause significant flow separations, increasing total roll damping. The equivalent damping rises with bilge keel height up to a critical point, after which it levels off. The distance between the bilge keel tip and the hull's center of rotation is crucial for roll damping and response amplitude. And also he revealed that the popular 45-degree installed bilge keel might not be the optimal configuration.

Walree [35] focused on evaluating deterministic and stochastic methods used to predict significant ship motions in severe weather conditions, including a comparison with Experimental Fluid Dynamics (EFD) data. The study was carried out as part of NATO AVT-280's initiative on "Evaluation of Prediction Methods for Ship Performance in Heavy Weather." The irregular waves are modeled based on the JONSWAP spectrum. Model tests recorded roll amplitudes of up to 40 degrees, and these were reasonably well predicted by panel methods. The EFD distribution of the roll angle exhibits a clear bimodal shape, effectively captured by Computational Fluid Dynamics (CFD). This observation confirms the resonance condition for roll motion, achieving substantial roll angles within the nonlinear regime.

Deng et al. [36] research on the viscous flow field around the transverse section of the Series-60 ship model with a bilge keel in the condition of forced rolling found that the vortex generated at the bilge keel during the rolling motion is the primary contributor of the rolling moment. He also discovered that the vortex formed by the bilge keel does not separate after falling off from the bilge keel, but is stretched into a slender vortex connected to the bilge keel. The stretched vortex is separated quickly when the hull moves in the reverse direction, and the vortex is shed from the bilge keel completely. The influence of the roll period and amplitude on the vortex structure in the flow field can be considered as the influence caused by the angular velocity. The characteristics of the vortex structures in the conditions of increasing roll amplitude of the same period and decreasing the period of the same amplitude are similar. The intensity of the generated vortex is increased with the roll angular velocity, and the outline of the generated vortex is susceptible to the enhanced interaction between it and the existing vortices, and the vortex is broken into several small scale vortices.

Another study conducted by Alexandersson et al. [37] to predict ship roll motions has been introduced, employing a hybrid method that integrates the Fully Nonlinear Potential Flow Method (FNPF) with the viscous damping principles derived from Ikeda's method. Through simulations of roll decay tests, the findings demonstrated a high level of concordance with corresponding scale model experiments. This method proves particularly valuable when accurate predictions of roll motions are essential, as these motions can not only impact other vessel movements through coupling effects but also result in exaggerated radiated waves. The hybridization of FNPF with Ikeda’s method, specifically the separation of viscous and inviscid roll damping, exhibited promising outcomes, particularly in the context of the KVLCC2 test case. Notably, a newly proposed regression formula for calculating sectional eddy damping showcased effectiveness by reproducing results from Ikeda's experiments. In the case of roll decay simulations for the KVLCC2, this regression formula performed significantly better when integrated into the hybrid method. These advancements contribute to more accurate predictions of roll motions in potential flow simulations and hold significance in understanding the interplay of various ship motions.

1.2. Thesis Objectives

This thesis focuses on a comprehensive parametric examination of the impact of bilge keels on roll damping for DTMB 5415 destroyer model. A computational procedure based on commercial CFD software (AQWA©) is applied to estimate the potential roll damping due to the radiated waves. The roll damping due to friction, eddy making, forward speed, and the bilge keel are estimated by using semi-empirical methods proposed by Ikeda [18].

The main objectives of this thesis can be summarized as follows :

- Development of a computational tool combining a commercial CFD software and a semi-empirical method to predict the roll damping of ships in regular waves,
- To demonstrate the effectiveness of the bilge keel on the roll damping by analyzing bilge keels with varying dimensions,
- To develop design recommendations for high speed displacement type vessels on the effectiveness of the bilge keel to reduce roll motion.

1.3. Contents of The Thesis

Chapter 2 describes the active and passive roll stabilization methods used for reducing the roll motion. The passive roll stabilization systems are classified as the bilge keels and passive anti-roll tanks while the active roll stabilization are classified as gyro systems, active anti-roll tanks, fin stabilizer systems and the rudder roll systems. The main design features as well as the advantages and disadvantages of these systems are presented. Chapter 3 covers the theoretical background theory of AQWA© which is a potential theory based commercial software developed and distributed by ANSYS. It is shown that this software neglects the viscous effects of the fluid and solves the Laplace equation with linearized free surface condition. The resulting damping is only due to the wave radiation and since the viscous effects are ignored an overestimated roll damping is expected.

In Chapter 4, analyses were conducted on cylindrical and rectangular structures to assess the accuracy of AQWA©'s wave-making effect calculations. The results of these analyses were compared with experimental data and results obtained from potential theory.

Chapter 5 presents the details of the semi-empirical method developed by Ikeda [18] to estimate the roll damping components due to the friction, eddy making, forward speed and the bilge keel which can not be estimated by AQWA©.

In Chapter 6, an analysis of the roll motion was performed by AQWA© on the DTMB 5415 model ship, and the results were compared with experimental data. Following this validation study, parametric analyses were conducted to investigate the effect of bilge keels of different sizes and angles on the roll motion.

2. STABILIZATION OF ROLL MOTION

The rolling movement of a vessel is a crucial factor in assessing its seakeeping capabilities. Excessive roll motion can restrict a ship's performance, and in extreme cases, it may lead to capsizing. Various methods can be employed to mitigate roll motion, and most of these methods involve counteracting the rolling movement. Since roll motion typically exhibits low inherent damping, increasing damping forces becomes a viable strategy to significantly reduce roll motion. This approach is particularly effective because maximum roll motion amplitudes tend to occur near the natural frequency.

Damping has the impact of gradually diminishing the free oscillation over time and adjusting the amplitude of the forced oscillation. In a perfectly regular sea, the ship would eventually oscillate exclusively within the wave periods. In real-world scenarios, the highest forced roll amplitudes tend to occur near the ship's natural frequency. This results in a ship at sea primarily oscillating at frequencies close to its inherent natural frequency. Thus, enhancing damping where the natural frequency aligns with high motion amplitudes, such as in the case of roll motion, proves to be more beneficial [38].

Barr [39] reccommends that once it's clear that a ship needs help with rolling, the designer has to pick the right stabilizer or a mix of them for that ship. According to Barr it's often a good idea to use different types, like bilge keels with either roll tanks or fins. He reccommends that this way, the ship gets the best help at both slow and fast speeds. Methods for roll stabilization can be categorized into active and passive approaches.

2.1. Passive Roll Stabilization

Passive roll stabilization is the use of devices or structures that do not require external power or control to reduce the rolling motion of a vessel. Passive roll stabilization has the advantage of being simple, reliable, and low-maintenance, as it does not depend on sensors, actuators, or software. However, passive roll stabilization also has some disadvantages, such as increasing the drag, weight, and cost of the vessel, and being

However, passive roll stabilization also has some disadvantages, such as increasing the drag, weight, and cost of the vessel, and being less effective at high speeds or in irregular waves [40].

2.1.1. Bilge keels

Bilge keels are small reinforced plates fixed on each side of the hull. They project outward in the bilge, approximately at the height where the hull turns. The primary function of bilge keels is to dampen the ship's roll motion. Some additional advantages, although of lesser importance, include acting as protection for the bilge area in case of grounding, increasing the longitudinal resistance of the hull structure at its level, and providing enhanced directional stability [41].

The bilge keel is usually positioned in the middle section of the ship's hull, often perpendicular to the turn of the bilge. The length of the bilge keel may be more than half the ship's overall length for large slow vessels but high speed vessels have shorter bilge keels due to the fineness of the underwater hull forms. When used in combination with active fin stabilizers the bilge keel may be arranged in two or three separate parts with fin stabilizers installed between them. Careful consideration of the precise placement of bilge keels on a ship is essential to maximize hydrodynamic roll resistance while minimizing forward motion resistance during sailing. Bilge keels are aligned with the flow streamlines around the ship when moving at its design speed in calm water. This minimizes their impact on increasing resistance to forward motion. Various positions and dimensions are typically tested during model tests to optimize its performance and, simultaneously, to calculate the power requirements for each option [42].

Designing bilge keels is crucial to ensure the integrity of the outer plates to which they are affixed. To prevent damage, thorough consideration is given to their shape, positioning, and the reinforced connection to the hull. To safeguard them, it is essential that the tips of the bilge keels are consistently positioned inside the ship's maximum beam and above the baseline. Extending beyond these limits would increase their vulnerability to potential damage during docking, dry-docking, and in shallow waters. Typical section of a conventional bilge keel is shown in Figure 2.1.

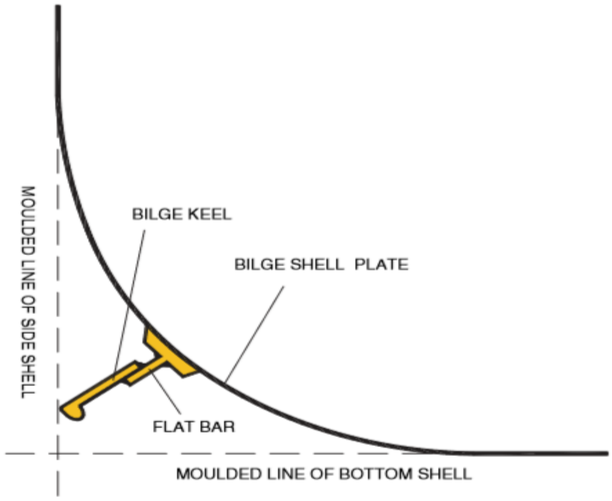

Figure 2.1 : Conventional bilge keel arrangement [41].

An alternative, though less common, approach involves a scalloped design along the entire length of the bilge keel. In this case, the keel may be directly welded to the hull using intermittent welds, forming a weak link with the hull. In larger vessels, the bilge keel typically adopts a transversal section with a 'V' shape, and it is internally reinforced at regular intervals. This design enhances the keel's structural integrity and overall effectiveness [41]. V type bilge keel presented in Figure 2.2.

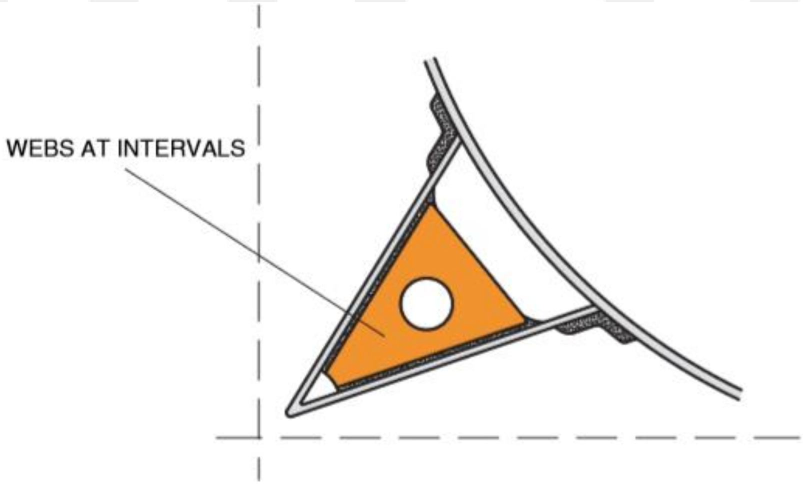

Figure 2.2 : Bilge keel section for a typical large vessel [41].

When the ship rolls, the bilge keel quickly takes in water, which scatters on the opposite side, creating eddies. While there is a minimal increase in added mass, there is a significant rise in damping effect due to the eddies and additional friction generated. The design of bilge keels incorporates a suitable profile and inclination to align with the flow streamlines when the ship is upright and in calm water conditions.

Many studies have demonstrated that roll damping increases linearly with increasing bilge keel span[43-44] . However, it has been shown that beyond a critical bilge span the damping effectiveness reduces as the generated vortices propagated away from the hull [45-47]. Research carried out by Ikeda [48] and Baniela [41] has shown that high-aspect-ratio bilge keels are most effective on slender ships, while the opposite is true for full ships.

Bilge keels offer a significant improvement in the roll damping compared to a ship without them, but their damping effect is smaller than that obtained by other roll stabilizing devices. However, because bilge keels are the only devices which can be used in very rough seas their installation is recommended whenever possible even though other stabilizing devices are set [41].

Rahmaji's [49] study show that the decision to include bilge keels on a ship depends on various factors, including the ship's size, purpose, and intended operating conditions. Generally, bilge keels become more advantageous as the size of the ship increases. Smaller vessels may not benefit as much from bilge keels, and there may be a length below which the advantages may be outweighed by the drawbacks. For smaller vessels such as yachts, pleasure boats, or small fishing boats, bilge keels might not be as common or necessary. The added drag and complexity may not justify the benefits in terms of stability for these smaller vessels.

2.1.2. Passive anti roll tanks

The first type of roll-stabilizing tank was suggested by W. Froude in his famous paper presented on reference [1]. In 1877, there were concerns about the stability of the HMS Inflexible, a Victorian battleship, because of new armor. Watts [50] tested a free surface tank on board the HMS Inflexible which was fitted in the available space. Despite the claims that the anti-roll tank reduced the roll angle some 20–25%, it was not effective. Frahm [50] designed and developed the U-type anti-roll tank. The design objective of this tank was that the tank should be in resonance with the natural roll period of the ship. However, Frahm wrongly assumed that the response of the tank would counteract the wave induced roll excitation, rather than acting as a damper.

These partially filled tanks consist of two wing tanks interconnected at the bottom through a substantial crossover pipe, when the ship initiates a rolling motion, the fluid moves from one tank to the other, generating a time-varying roll moment that is carefully designed to be in the correct phase, thereby reducing the vessel's roll motion. The effectiveness of the stabilizing moment depends on factors such as the size and location of the roll damping tank, as well as the hull form and loading condition of the vessel. The motion equation for the liquid in the tank is derived based on two simplifying assumptions [51]:

1. The liquid's relative motion within the system is assumed to be one-dimensional.
2. The coupling between 6DOF equations governing the motion of the ship and the motion of the tank liquid occurs exclusively through the roll motion.

Nevertheless, due to the inherent coupling within the equations of motion for the ship, there exist indirect interactions between the motion of the tank liquid and the other degrees of freedom. For a purely roll motion the following equation used.

$$\mathrm{A}_{44}\ddot{\phi} + \mathrm{b}_{44}\dot{\phi} + \mathrm{c}_{44}\phi + [\mathrm{a}_{4\alpha}\ddot{\alpha} + \mathrm{c}_{4\alpha}\alpha] = F\sin(\omega_{\mathrm{e}}t) \tag{2.2}$$

where ϕ is the roll angle of the ship, $\dot{\phi}$ is roll velocity of ship, $\ddot{\phi}$ is roll acceleration of ship, A_{44} is the ship roll inertia, b_{44} is the ship roll damping coefficient, c_{44} is the ship roll stiffness, F is the amplitude of the excitation roll moment, ω_{e} is the wave encounter frequency, α is the angle of the water surface in the tank and $\ddot{\alpha}$ is acceleration of water column.

$\mathrm{a}_{4\alpha} = \mathrm{Q}_{\mathrm{t}}(\mathrm{r}_{\mathrm{d}} + \mathrm{h}_{\mathrm{r}})$

$\mathrm{c}_{4\alpha} = \mathrm{Q}_{\mathrm{t}}g$

and $\mathrm{Q}_{\mathrm{t}} = 0.5\rho_{\mathrm{t}}\mathrm{w}_{\mathrm{r}}\mathrm{w}^2\mathrm{x}_{\mathrm{t}}$ where x_{t} is the length of the tank

The expression inside the square brackets is the roll stabilizing moment from the liquid inside the tank. The tank natural frequency ω_t is given by

$$\omega_{\mathrm{t}} = \sqrt{\frac{2\mathrm{g}\mathrm{h}_{\mathrm{d}}}{\mathrm{w}_{\mathrm{r}}\mathrm{W} + 2\mathrm{h}_{\mathrm{r}}\mathrm{h}_{\mathrm{d}}}} \tag{2.3}$$

which depends on the tank dimensions and gravitational acceleration g. This information is applied in the tank tuning process in applications. $\mathrm{h}_{\mathrm{r}}, \mathrm{h}_{\mathrm{d}}, \mathrm{w}_{\mathrm{r}}, \mathrm{W}$ described in Figure 2.3. Tank tuning is a process that damping effect is maximized by approaching $\mu_{\mathrm{t}} = \frac{\mathrm{w}_{\mathrm{t}}}{\mathrm{w}_{\mathrm{s}}} = 1$ [52].

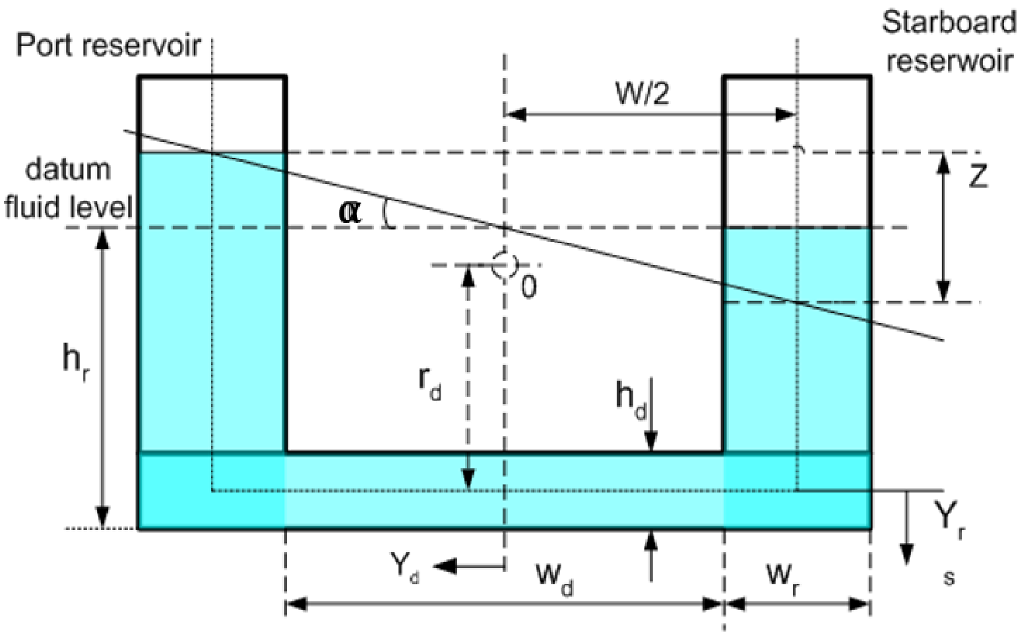

Figure 2.3 : Passive anti-roll tank its geometric parameters [51].

Passive anti roll tanks do not impede the fore and aft passage, as there is available space above and below the water-crossover pipe for other purposes. Passive anti roll tanks can work efficiently at zero speed. Typically, a passive roll damping tank can achieve an average roll reduction ranging from 40% to 60% [53]. Their simplicity and lack of reliance on external power make them easy to maintain. The natural movement of water within the tanks provides effective roll stabilization, contributing to passenger and crew comfort. However, passive anti roll tanks may be less effective in extreme conditions because of lack real-time adaptability.

2.2. Active Roll Stabilization

Active roll stabilization employs dynamic control systems or electronic mechanisms to actively mitigate and reduce the rolling motion of a vessel. This approach depends on real-time sensing and feedback systems to dynamically regulate and maintain the vessel's stability, responding actively to disturbances that might initiate rolling.

2.2.1. Gyroscopes

Gyro stabilizers can be installed internally within the ship, utilizing gyroscopic forces to minimize the rolling motion. Importantly, it operates without the need for a dedicated controller or a device to measure the ship's roll motion.

A spinning flywheel generates angular momentum that extends at a right angle to the rotation plane. Angular momentum, being a vector quantity, follows a specific direction determined by the right-hand rule, as illustrated in Figure 2.4.

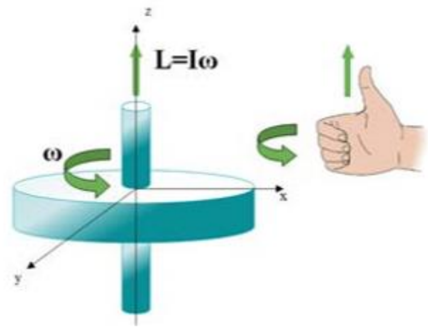

Figure 2.4 : Angular momentum of rotating flywheel [54].

Angular momentum is the product of moment of inertia, *I* and angular velocity, ω.

$$\vec{L} = I\vec{\omega} \tag{2.4}$$

Stabilizing torque of gyroscope is generated through a simultaneous three-step process [54].

1. The vessel experiences rolling due to sea waves, which can be depicted as a force F_x acting along the x-axis. Concurrently, the gyroscope rotates in a counterclockwise direction, generating angular momentum along the z-axis.
2. The gyroscope rolls alongside the boat, firmly attached to the roll axis. It exhibits an angular velocity ω_x due to the boat's rolling motion. This angular velocity, in turn, generates a moment M_y along the y-axis, as depicted in Figure 2.5. The moment M_y leads to a change in direction ΔL in angular momentum, causing the gyroscope to pivot along the y-axis. This motion is termed the precession of the gyroscope, with L_1 representing the resultant angular momentum.

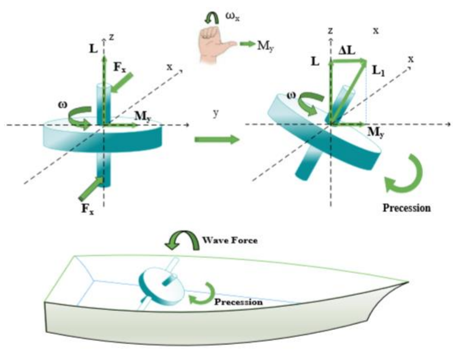

Figure 2.5 : Change of angular momentum of the gyroscope [54].

3. The gyroscope exhibits an angular velocity ω_y due to the precession motion. This angular velocity gives rise to a momentum M_x perpendicular to its direction, as illustrated in Figure 2.6. The angular velocity ω_y reaches its maximum value at the onset of the precession motion, leading to a corresponding peak in M_x at that time. The combined effects of M_x and L_1 yield a stabilizing moment M_s. This stabilizing moment, occurring in the same plane but in the opposite direction of the roll motion, acts as a resistance against the forces induced by sea waves. This stabilizing moment coincides with the precession motion, contributing to the overall stability of the system.

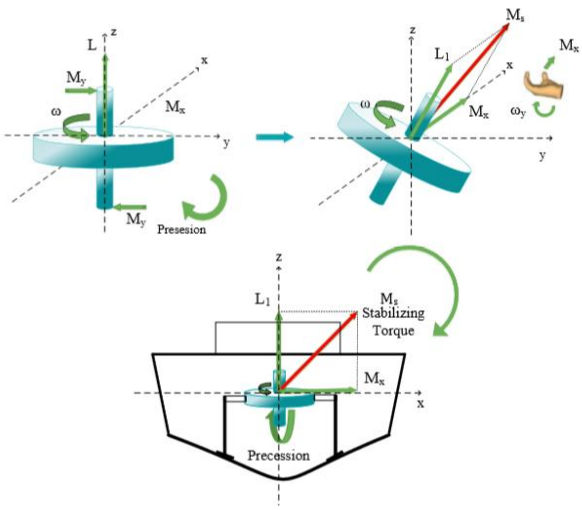

Figure 2.6 : Creation of stabilizing moment [54].

The concept of utilizing gyroscopic stabilizers was initially proposed by Schlick in 1904, with similar suggestions put forth by Brennan and Forbes in 1903 and 1904 respectively [55]. This idea saw its first practical implementation on a German torpedo boat in 1906. Subsequently, in 1909, a prototype gyro was manufactured in Washington for stabilization purposes, which was then installed on the US Destroyer Worden [55]. Active stabilization systems have been in development since 1912, finding application across various sectors. Private yachts began adopting gyroscopic stabilizers later on. Gyroscopic stabilization has been and continues to be implemented on numerous civilian, military, as well as small and medium-sized vessels worldwide. Typically, gyroscopes can mitigate approximately 60% to 90% of the boat's rolling and trimming movements [55]. Advantages of gyroscopes, as highlited in Alaswad's study [56] include the reduction of both rolling and pitching motions significantly for yachts.

These gyro stabilizers can be effectively deployed within a broad range of motion, spanning from 30 to over 100 degrees, and they prove efficient whether the yacht is anchored or docked. Moreover, they contribute to smoother cruising experiences at higher speeds without necessitating additional external devices to reduce drag. Additionally, their versatility is evident in their ability to come in various sizes and configurations, adapting to different yacht layouts [56].

On the other hand, the study of Alaswad notes several disadvantages: gyroscopes may take 30-45 minutes to reach their operational speed, and their considerable space requirements pose challenges for installation within yacht interiors. Furthermore, improper mounting can lead to significant damage, necessitating correct placement on the yacht's stringers. Ensuring proper stringer reinforcement installation by the manufacturer is crucial to avoid potential issues [56].

2.2.2. Active anti roll tanks

Active anti roll tank systems consist of two symmetrical vertical side tanks similar to U-type passive anti roll tanks but fitted with pumps in the central channel to facilitate the movement of water between vertical tanks. The system's operation is determined by a controller, which calculates the required actions based on the ship's motion as detected by motion sensors. The efficiency of activated tank systems relies heavily on factors such as tank geometry, pump power, and control methodologies. Typically, the ideal tank configuration is chosen early in the design process, considering power supply and spatial considerations on the ship. As a result, the design of the controller becomes a critical factor influencing the overall efficiency of the system [57].

The fluid tank is located amidships to generate the antiroll moment by fluid movement. In the central channel of the tank, a variable-pitch impeller is installed to control the velocity and direction of tank flow. On the contrary of passive roll tanks, active roll tanks are useful as well if the rolling rhythm of the vessel doesn't align with the intended oscillation pattern of the fluid in the tank [58]. Active anti-roll tank shown in Figure 2.7.

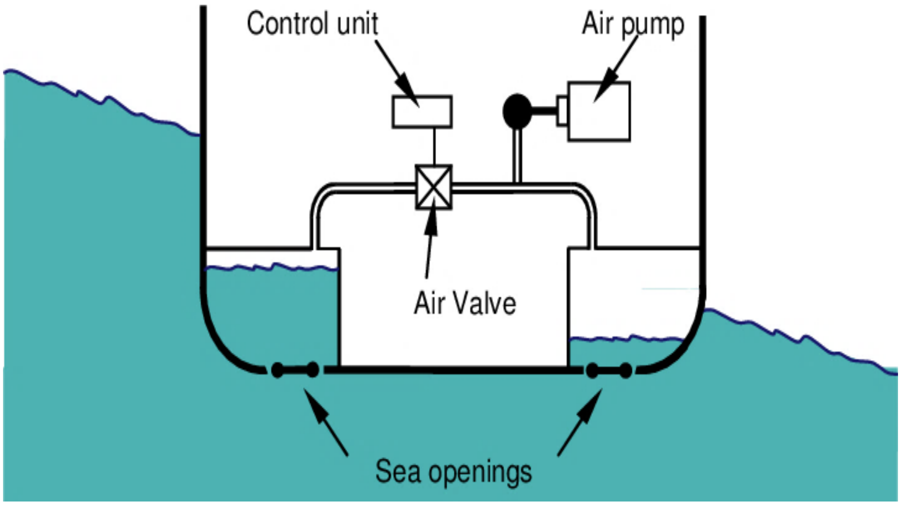

Figure 2.7 : Active Anti-Roll Tank [57] .

The concept of activated antiroll tanks emerged in 1928 as a means to enhance stabilization efficiency. The first full-scale implementation occurred on a US destroyer. Over time, various iterations of activated tank systems were developed and put into practical use [59].

Marzouk [60] studied a comparison of undamped, active and passive anti roll tanks by means of roll damping efficiency for ships like cargo ships. Marzouk claimed that both active and passive anti roll tanks helps to decrease roll damping. Active anti roll tanks more are efficient compared to passive anti roll tanks in roll damping. Anti roll tanks can be used in lower or zero speeds just as in passive anti roll tanks. Their widespread use is limited, particularly in warships, due to the significant space requirements they entail [61]. As can seen in the study in reference [60], a well-thought-out design incorporates an optimal active controlling to diminish water movements at resonance and broaden the frequency range over which the tank operates effectively [62].

In order to design an effective controller for an active antiroll tank system, it is necessary to have a reliable dynamic model of the ship roll and tank flow motion. The primary goal of the active anti roll tank design is to establish an appropriate tuning law that minimizes the rolling motion to a reasonable level while ensuring the impeller operates in a rational manner. Applying this principle, we can establish a performance index that quantifies both the effectiveness in reducing rolling motion and the associated power consumption.

2.2.3. Active fin stabilizers

Active fin roll stabilizers are designed to minimize a ship's rolling motion caused by wave action or external forces. The fundamental working principle involves a combination of sensor input, control systems, and dynamic fin movement. Sensors, such as gyroscopes and accelerometers, continuously monitor the ship's roll, pitch, and yaw movements. This real-time data is processed by a control system, which calculates the necessary corrective actions to counteract the rolling motion. The control system then directs hydraulic actuators to adjust the position and angle of fins located beneath the waterline. These fins rapidly move in response to the control signals, generating hydrodynamic forces that act against the rolling motion of the ship [63]. By dynamically altering the orientation of the fins based on the ship's movement, active fin roll stabilizers effectively damping the rolling motion and enhance the vessel's stability. Typical active fin stabilizer on a cruis ship presented in Figure 2.8.

Figure 2.8 : Typical active fin stabilizer on a cruise ship [64].

From a fluid dynamics perspective, when a fin moves through a fluid, it experiences a drag force resulting from pressure differences and frictional stress. Additionally, there's a viscous pressure drag, known as vortex drag, generated by the fluid's motion in the boundary layer over the fin surface.

The optimum fin area is calculated based on the wave slope capacity of the fin. Wave slope capacity is the hull heel angle caused by the maximum lift force of the fin in calm sea [65].

$$\beta_{wsc} = \sin^{-1}\left(\frac{FL}{\Delta GM_T}\right) \tag{2.5}$$

Where F is fin lift force and L is the moment of arm lever. GM_T is transverse metacentric height and Δ is displacement.

Fin area based on wave slope capacity A_f

$$A_f = \frac{\Delta GM_T sin\beta_{wsc}}{\rho C_L v^2 L} \tag{2.6}$$

C_L is the coefficient of lift and v is ship speed. ρ is density, L is the moment of arm lever.

Design recommendations about fin stabilizers are described by Lloyd [66];

a. Fin Location:

Optimize stability by placing the fins near the middle of the ship's turn of the bilge. Avoid mounting bilge keels behind the fins. Bilge keels create hydrodynamic drag as water flows around them. When positioned behind the fins, bilge keels can increase the drag already generated by the fins, and it can effect the stability and rolling of ship in negative way. Ensure the fins are perpendicular to the hull surface without extreme angles, particularly for aft-mounted fins.

b. Fin Size and Shape:

Aim for maximum stability with fins as large as possible. For fixed fins, ensure they fit within a rectangle defined by the ship's maximum beam and draught. Maintain an aspect ratio of fins above 1, and position the fin stock at the quarter chord for reduced torque requirements. Choose a symmetrical section with ample thickness to support the necessary stock diameter.

c. Number of Fins:

Preferably use a single pair of fins to minimize interference effects. Only consider employing a two-fin configuration if a single pair does not provide adequate stabilization. If necessary, optimize the longitudinal separation between fins to capitalize on favorable interference effects.

Forces acting on a fin as shown in Figure 2.9 can be calculated as follows;

$$P = \sqrt{P_y^2 + P_x^2} = \sqrt{P_n^2 + P_t^2} \tag{2.7}$$

$P_n = P_y \cos\alpha + P_x \sin\alpha$

$P_t = P_x \cos\alpha + P_y \sin\alpha$

$M_r = P_n(e - d)$

$M = P_n e$

α: Angle of attack

e: Distance to midpoint of fin chord

d: Distance to fin shaft

M_r: Axis fin moment is the torque exerted on the vessel's hull by the fins to counteract rolling motion.

M: Attack moment is the torque created by the angle of attack of the fins relative to the direction of motion of the vessel.

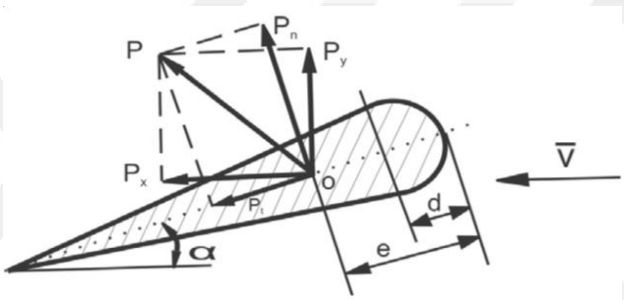

Figure 2.9 : Fixed fin stabilizer forces [53].

Gatzoulis [67] stated that the amount of roll reduction that can be expected by using fins is a function of a given ship's size, number and size of fins, design of fin controller, ship speed, heading and the existing sea conditions.

For properly designed systems, and with a ship speed of approximately 12 knots or greater, roll reductions from about % 50 to 95 can be expected at most headings in various seaways . In another study, Patil [65] studied on efficiency of fin stabilizers and results claim that above 12 knots, efficiency of fin stabilisers are around %90. However, fin stabilizers exhibit suboptimal performance during low-speed maneuvers or when a ship is anchored [68].

2.2.4. Rudder roll stabilization

The rudder's main role is to control the yaw motion, influencing the ship's heading during maneuvers like coursekeeping or course-changing. However, a noticeable inward roll occurs shortly after initiating a turning maneuver, attributed to the rudder's not turning enough. The concept of rudder roll stabilizers (RRS) leverages this inward roll induced by the rudder to mitigate the associated high-frequency wave-induced roll motion. In contrast to heading control autopilots, which primarily focus on compensating for low-frequency yaw motion, RRS prioritizes reducing high-frequency roll induced by waves. To achieve effective roll reduction without disrupting the ship's heading control, it is crucial for the bandwidth of the rudder roll control system to be higher than that of the rudder yaw control system. This necessity implies that the rudder slew rate limit must be sufficiently high to achieve satisfactory roll reduction performance. Therefore, the objective of RRS differs from heading control autopilots, placing emphasis on mitigating high-frequency wave-induced roll rather than addressing low-frequency steady-state heeling [35]. Rudder roll stabilizer rolling force diagram presented on Figure 2.10.

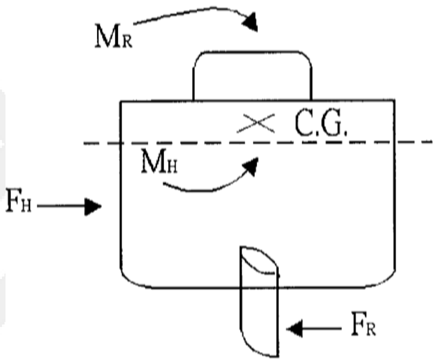

Figure 2.10 : Rudder roll induced rolling force diagram [69].

Referring to Figure 2.10, the rudder-induced force, F_R becomes evident immediately upon the rudder reaching the starboard position. This force generates a clockwise moment, M_R, inducing an inward roll of the ship. It's important to note that the rudder-induced force, F_R, also leads to a sideway kick phenomenon. Due to the significant size difference between the ship and the rudder, the hull-induced force, F_H, gradually builds up as a result of the drift angle. Once F_H comes, a counterclockwise moment, M_H, is generated, surpassing the rudder-induced moment M_R and causing an outward roll. As the ship progressively rolls outward, a restoring moment is activated to counteract the moment induced by the hull force, M_H. Eventually, the ship reaches a steady outward roll angle when the restoring moment equals but opposes the hull force induced moment M_H. The inward roll phenomenon caused by the rudder moment M_R is strategically employed to mitigate the roll motion of a ship navigating in seaways [69].

Fin stabilizers and active anti-roll tanks often incorporate complicated mechanisms, requiring additional space. As a result, an alternative approach that leverages existing equipment onboard, such as the ship's rudder, appears to be highly appealing.

The primary challenge in the rudder roll stabilization system stems from the constraints imposed by the limited rudder angle and rudder rate. Inadequate management of these factors can lead to a deterioration in performance and may even result in system instability. Proper attention and care are crucial to address these limitations effectively. Baitis [70] reported achieving a 50% roll damping effect by using rudder roll stabilization on a destroyer. Santoso [71] stated that efficiency of rudder roll is up to %50-%70. Sgobbo [72] studied on efficiency of rudder roll stabilization on USCG WMEC 901 class vessel. In his study, he claimed that rudder stabilization may reduce damping up to %55 approximately.

The following table presents a comparison of roll stabilization methods for commercial and military ships in terms of initial installation cost [73], maintenance cost [73], efficiency [73] and damping ratio. [74] Bilge keels stand out as the predominant stabilizing technique among both active and passive roll stabilization methods, as highlighted in reference. Their widespread preference is attributed to the combination of low initial installation and maintenance costs, coupled with a relatively high level of efficiency. These characteristics positions bilge keels as a favorable choice when compared to other systems for roll stabilization. Comparison of roll damping methods for naval ships given in Table 2.1. Damping ratio in Table 2.1 given according to naval ships.

Table 2.1 : Comparison of roll damping methods for naval ships.

Roll Prevention Method	Bilge Keels	Active Anti Roll Tanks	Passive Anti Roll Tanks	Fin Stabilizers	Rudder Roll Damping
Damping Ratio [74]	%15, >%35	%70 [75]	%40	%90	%50
Initial Installation Cost [73]	Low	High	Medium	High	Medium
Maintenance Cost [73]	Low	High	Medium	High	Medium
Efficiency [73]	Medium	High	Medium	High	Medium

3. BACKGROUND THEORY OF AQWA©

AQWA© can simulate linearized hydrodynamic fluid wave loading on floating or fixed rigid bodies. It achieves this by utilizing advanced mathematical theories like three-dimensional radiation/diffraction theory and Morison's equation within the frequency domain, particularly in regular wave conditions. Additionally, AQWA© can conduct detailed analyses of how structures behave under the combined influences of hydrostatic and hydrodynamic forces in varying wave conditions within the frequency domain [76].

AQWA© offers the capability to analyze the dynamic responses of floating structures in irregular wave environments, specifically in the frequency domain. It can handle both coupled and uncoupled responses, providing insights into how different parts of the structure interact with each other under varying wave conditions.

The real-time motion of a floating body or bodies while operating in regular or irregular waves can be simulated, in which nonlinear Froude-Krylov and hydrostatic forces are estimated under instantaneous incident wave surface. Additionally, the real-time motion of a floating body or bodies while operating in multi-directional or unidirectional irregular waves can be simulated under first- and second-order wave excitations [76] .

3.1. Hydrodynamic Radiation and Diffraction Analysis by Source Distribution Method

Hydrodynamic loading on a marine structure is mainly caused by the kinematics of water particles in waves, motions of the structure and interactions between waves and the structure [76].

Drag loads are induced by viscosity and are proportional to the square of relative velocity between fluid particle and structure surface. They are important when structural members are slender and wave amplitude is large [76]. In small amplitude waves, the wave exciting load consists of the first order incident wave force (Froude-Krylov force) and the diffraction force which is induced by the disturbance wave due to the existence of a body. In larger seas, both the first order forces and the second order forces are important. In severe seas, bottom and flare slamming transient forces may also be included [76].

Wave inertia load or radiation load is caused by the disturbed waves induced by the body motions. Fluid potential theories are commonly used for solving the wave inertia load and wave exciting load [76].

Three dimensional panel methods are the most common numerical tools to analyze the hydrodynamic behavior of a large-volume structure in waves. These methods are based on the fluid potential theory and represent the structure surface by a series of diffraction panels. The Morison's equation approach is widely used for slender body components. AQWA© employs a hybrid method to model the large-volume components of a structure by diffracting panels and the small cross sectional components by Morison elements [76].

3.1.1 Radiation and diffraction wave forces

The main theoretical assumptions and limitations of linear potential theory employed in AQWA© are listed below:

• The fluid is inviscid and incompressible, and the fluid flow is irrotational.

• The incident regular wave train is of small amplitude compared to its length (small slope).

•The motions are to the first order and hence must be of small amplitude. All body motions are harmonic. The linearized drag damping on the Morison elements or any additional user-defined viscous damping can be optionally included in the equation of motion [76].

3.1.2. Source distribution method

By assuming the fluid ideal such that there exists a velocity potential function with isolated space dependent term and employing linear hydrodynamic theory, accounting for wave radiation and diffraction, the fluid-structure interaction behavior is described by the following set of equations in the fixed reference axes [76]:

• Laplace equation:

$$\Delta\phi = \frac{\partial^2\phi}{dx^2} + \frac{\partial^2\phi}{dy^2} + \frac{\partial^2\phi}{dz^2} = 0 \tag{3.1}$$

applicable everywhere in the fluid domain. Here, x y, z represents the direction of the velocity and ϕ is velocity potential.

• Linear free surface equation of zero forward speed case:

$$-\omega^2\phi + \frac{\partial\phi}{\partial z} = 0 \text{ on } z = 0 \tag{3.2}$$

Where ω is

• Body surface conditions:

$$\frac{\partial\phi}{\partial n} = \begin{cases} -i\omega n & \text{for radiation potential} \\ -\dfrac{\partial\phi}{\partial n} & \text{for diffraction potential} \end{cases} \tag{3.3}$$

• Seabed surface condition at depth of d :

$$\frac{\partial\phi}{\partial z} = 0 \text{ on } z = -d \tag{3.4}$$

• A suitable radiation condition must be added to these equations so that as $\sqrt{(x^2 + y^2)} \rightarrow \infty$ the generalized wave disturbance dies away.

A boundary integration approach is employed in AQWA© to solve the fluid velocity potential governed by the above control conditions. In this approach the frequency domain pulsating Green's function in finite depth water is introduced, which obeys the same linear free surface boundary condition, seabed condition, and far field radiation conditions as those given in equation 3.2 and equation 3.4 [76].

Using Green's theorem, the velocity potential of diffraction and radiation waves can be expressed as in equation 3.5.

$$c\phi(\vec{X}) = \int_{s_0} \left\{ \phi(\vec{\varsigma}) \frac{\partial G(\vec{X}, \vec{\varsigma}, \omega)}{\partial n(\vec{\varsigma})} - \partial G(\vec{X}, \vec{\varsigma}, \omega) \frac{\partial \phi(\vec{\varsigma})}{\partial n(\vec{\varsigma})} \right\} dS \tag{3.5}$$

where

$$c = \begin{cases} 0 & \vec{X} \notin \Omega \cup S_0 \\ 2\pi & \vec{X} \in S_0 \\ 4\pi & \vec{X} \in \Omega \end{cases} \qquad \Omega : \text{Fluid domain}$$

$\vec{X} = (X, Y, Z)$ is the location of a point on the submerged body surface. S_0 is submerged body surface. $\vec{\varsigma}$ denotes the position of a source.

The source distribution over the mean wetted surface, the fluid potential is given in equation 3.6.

$$\phi(\vec{X}) = \frac{1}{4\pi} \int_{S_0} \sigma(\vec{\varsigma})\, G(\vec{X}, \vec{\varsigma}, \omega) dS \text{ where } \vec{X} \in \Omega \cup S_0 \tag{3.6}$$

where $\sigma(\vec{\varsigma})$ is unknown source strength. To obtain the source strength over the mean wetted surface, kinematic boundary condition of oscillating body can be applied:

$$\frac{\partial \phi(\vec{X})}{\partial n(\vec{X})} = -\frac{1}{2}\sigma(\vec{X}) + \frac{1}{4\pi} \int_{S_0} \sigma(\vec{\varsigma}) \frac{\partial G(\vec{X}, \vec{\varsigma}, \omega)}{\partial n(\vec{X})} dS \quad \text{where } \vec{X} \in S_0 \tag{3.7}$$

where n is the normal vector of the hull. To solve the above equation, in which the mean wetted surface of a floating body is divided into quadrilateral or triangular panels in AQWA© as shown in Figure 3.1. It is assumed that the potential and the source strength within each panel are constant and taken as the corresponding average values over that panel surface.

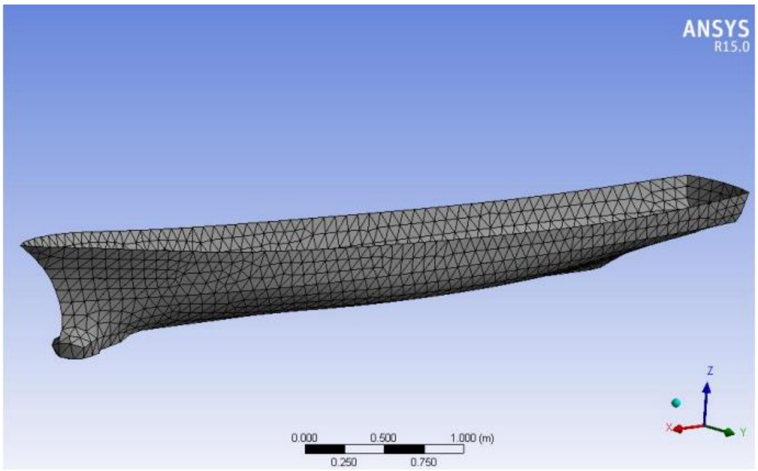

Figure 3.1 : Panel model of DTMB 5415 in AQWA©.

3.2. Dynamics of Floating Bodies

A floating object experiences two distinct forces when subjected to regular waves in a inviscid environment. The first force is the hydrostatic restoring force, while the second force arises from the interaction with the incident waves, termed as the hydrodynamic force. Initially, the forces exerted by the incident waves are computed by evaluating the dynamic pressure acting on the submerged surface area. The total dynamic pressure is defined using the linearized Bernoulli equation, and the corresponding forces are derived by integrating the pressure across the wetted surface. Subsequently, the inertial forces (inclusive of added mass) and damping forces are evaluated upon obtaining the radiation potential.

The velocity potential of the fluid around the floating body is defined as

$$\phi(x, y, z, t) = \zeta_a \phi(x, y, z) e^{-i\omega_e t} \quad (3.8)$$

where ζ_a represents wave amplitude and ω_e represents encounter frequency. The encounter frequency is defined as:

$$\omega_e = \omega - \frac{\omega^2 U}{g} \cos\beta \quad (3.9)$$

where β and U are wave heading and velocity. The velocity potential $\phi(x, y, z)$ can be divided into incident potential, diffraction potential and radiation potential which is caused by the oscillation of body in six degree of freedom. All these three potentials have complex characters.

$$\phi(x, y, z) e^{-i\omega t} = [(\phi_I + \phi_D) + \sum_{6}^{j=1} \phi_{Rj} x_j] e^{-i\omega t} \quad (3.10)$$

where ϕ_I the first order incident wave potential, *D* is the diffraction wave potential and ϕ_{Rj} is the radiation wave potential caused by j^{th} motion.

The translational and rotational motions of the body in the unit amplitude regular incident waves can be written as shown in Table 3.1.

Table 3.1 : Motion, velocity and force/moment components.

Mode	Motion	Axis	Force / Moment	Motion	Velocity	Acceleration
1	Surge	x	X	η_1	$\dot{\eta}_1$	$\ddot{\eta}_1$
2	Sway	y	Y	η_2	$\dot{\eta}_2$	$\ddot{\eta}_2$
3	Heave	z	Z	η_3	$\dot{\eta}_3$	$\ddot{\eta}_3$
4	Roll	θ	K	η_4	$\dot{\eta}_4$	$\ddot{\eta}_4$
5	Pitch	ϕ	M	η_5	$\dot{\eta}_5$	$\ddot{\eta}_5$
6	Yaw	ψ	N	η_6	$\dot{\eta}_6$	$\ddot{\eta}_6$

Since the velocity potential of the wave is obtained, the first-order hydrodynamic pressure distribution can be calculated utilizing the linearized Bernoulli equation:

$$p^{(1)} = \rho[i\omega_e \phi(x,y,z) + \vec{U}\nabla\phi(x,y,z)]e^{-i\omega_e t} \tag{3.11}$$

Forces induced by waves can be calculated by integration of pressure on wetted surface. To represent the forces and moments in general form, the unit normal vector is defined in six degree of freedom as below:

$$(n_1, n_2, n_3) = \vec{n} \text{ and } (n_4, n_5, n_6) = \vec{n} \times \vec{r} \tag{3.12}$$

Where $\vec{r} = \vec{X} - \overrightarrow{X_g}$ represents the position vector. It is the location of any point on wetted surface according to the structure's center of gravity.

First order hydrodynamic forces and moments are expressed by below general formula with this notation:

$$F_j e^{-i\omega t} = -\int_{s_0} p^{(1)} n_j dS = -\rho \int_{s_0} [(i\omega_e + \vec{U}\nabla)\phi(x,y,z)]n_j dS \tag{3.13}$$

Where S_0 represents the wetted surface of the structure.

The total first order hydrodynamic forces are written as below:

$$F_j = [(F_{Ij} + F_{dj}) + \sum_{k=1}^{6} F_{rjk} x_k] \quad j = 1,6 \tag{3.14}$$

j^{th} Froude-Krylov force due to incident wave:

$$F_{Ij} = -\rho \int_{s_0} [(i\omega_e + \vec{U}\nabla)\phi_I(x,y,z)]n_j dS \tag{3.15}$$

j^{th} diffraction force due to diffracted wave:

$$F_{dj} = -\rho \int_{s_0} [(i\omega_e + \vec{U}\nabla)\phi_d(x, y, z)]n_j dS \tag{3.16}$$

j^{th} radiation force due to unit amplitude rigid motion of k^{th}: [76]

$$F_{rjk} = -\rho \int_{s_0} [(i\omega_e + \vec{U}\nabla)\phi_{rk}(x, y, z)]n_j dS \tag{3.17}$$

The radiated waves are caused by oscillation of the floating body in still water. Radiated waves are strongly related to the hydrodynamic characteristics of the body. Therefore, real and imaginary parts of the radiation potential ϕ_{rk} are used in order to calculate the added mass and radiation damping of the body in induced wave frequency:

$$A_{jk} = \frac{\rho}{\omega_e^2} \iint_{S_0} Re[(i\omega_e + \vec{U}\nabla)\, \phi_{rk}(x, y, z)]n_j dS \tag{3.18}$$

$$B_{jk} = -\frac{\rho}{\omega_e} \iint_{S_0} Re[(i\omega_e + \vec{U}\nabla)\, \phi_{rk}(x, y, z)]n_j dS \tag{3.19}$$

3.3. Roll Motion In Regular Waves

If we assume that a ship rolls about her center of mass which is usually close to the undisturbed water line then dynamics are described by the equation [76] :

$$[\, J_{xx} + I_{\varphi\varphi}(\omega)]\ddot{\varphi} + N_{\varphi\varphi}(\omega)\dot{\varphi} + C_{\varphi\varphi}\varphi = K_{\varphi}(t) \tag{3.20}$$

where:

$K_{\varphi}(t)$ is a sinusoidal mechanical excitation producing a rolling moment

φ is the angle of roll

J_{xx} is the mass moment of inertia about the longitudinal axis through the centre of mass

$C_{\varphi\varphi}$ is hydrostatic roll restoring coefficient

$I_{\varphi\varphi}$ is roll added inertia

$N_{\varphi\varphi}$ roll damping coefficient

It is observed that as a ship moves forward, the damping effect on roll motion increases. This increase in damping leads to a reduction in the maximum resonant peak, though accompanied by a slight decrease in the frequency at which this peak response occurs. The mass of a ship is determined by its overall weight or displacement. Consequently, the rotational inertia related to roll motion depends on the distance of each weight from the ship's center of gravity (CG). The farther the heaviest weights are from the CG, the greater the rotational moment of inertia. If all of the masses were located equidistant from the center of gravity, the moment of inertia would be easy to calculate and would be equal to the total mass times the distance from the CG squared. To consider roll damping viscous effects to the motion, see Chapter 5.

3.4. Response Amplitude Operators

AQWA© computes the response of a body to regular waves by solving a series of linear algebraic equations. These equations represent the motion of the body in response to hydrodynamic interactions, with coefficients that vary with frequency. The resulting characteristics, known as Response Amplitude Operators (RAOs), describe how the body responds to waves and are directly related to the wave amplitude. The set of linear motion equations of hydrodynamic interaction structures with frequency dependent coefficients are obtained by equation below [76]:

$$\left(-\omega^2[M + A(\omega)] + i\omega[B(\omega) + B_v] + [C]\right)X = F(\omega) \tag{3.21}$$

M: mass matrix

$$\begin{bmatrix} m & 0 & 0 & 0 & 0 & 0 \\ 0 & m & 0 & 0 & 0 & 0 \\ 0 & 0 & m & 0 & 0 & 0 \\ 0 & 0 & 0 & I_x & 0 & 0 \\ 0 & 0 & 0 & 0 & I_y & 0 \\ 0 & 0 & 0 & 0 & 0 & I_z \end{bmatrix}$$

where m is mass of the ship.

A: added mass matrix

$$\begin{bmatrix} A_{11} & A_{12} & A_{13} & A_{14} & A_{15} & A_{16} \\ A_{21} & A_{22} & A_{23} & A_{24} & A_{25} & A_{26} \\ A_{31} & A_{32} & A_{33} & A_{34} & A_{35} & A_{36} \\ A_{41} & A_{42} & A_{43} & A_{44} & A_{45} & A_{46} \\ A_{51} & A_{52} & A_{53} & A_{54} & A_{55} & A_{56} \\ A_{61} & A_{62} & A_{63} & A_{64} & A_{65} & A_{66} \end{bmatrix}$$

B: Damping matrix

$$\begin{bmatrix} B_{11} & B_{12} & B_{13} & B_{14} & B_{15} & B_{16} \\ B_{21} & B_{22} & B_{23} & B_{24} & B_{25} & B_{26} \\ B_{31} & B_{32} & B_{33} & B_{34} & B_{35} & B_{36} \\ B_{41} & B_{42} & B_{43} & B_{44} & B_{45} & B_{46} \\ B_{51} & B_{52} & B_{53} & B_{54} & B_{55} & B_{56} \\ B_{61} & B_{62} & B_{63} & B_{64} & B_{65} & B_{66} \end{bmatrix}$$

C: Hydrostatic restoring force matrix

$$\begin{bmatrix} 0 & 0 & 0 & 0 & 0 & 0 \\ 0 & 0 & 0 & 0 & 0 & 0 \\ 0 & 0 & C_{33} & C_{34} & C_{35} & 0 \\ 0 & 0 & C_{43} & C_{44} & C_{45} & C_{46} \\ 0 & 0 & C_{53} & C_{54} & C_{55} & C_{56} \\ 0 & 0 & 0 & 0 & 0 & 0 \end{bmatrix}$$

Hydrostatic restoring forces are the forces when the structure returns to static position while moving in waves and independent of wave frequencies. Restoring force for roll motion can be calculated as below [76]:

$$C_{44} = \rho g A_{xx} + Mg(z_b - z_G) = \rho g V GM_T \tag{3.22}$$

where,

A_{xx} second moment of inertia of waterline area, z_b is the position of center of buoyancy and z_G is the position of center of gravity, V is volumetric displacement of floating body.

Mass matrix, added mass matrix and hydrostatic restoring force matrices are the outcome of AQWA© [76].

4. ROLL MOTION PREDICTION by AQWA©

The wave making damping due to the roll motion for two dimensional sections at zero forward speed can be estimated with sufficient accuracy by theoretical methods based on the potential theory, such as the conformal mapping [77] and Frank Close-Fit [78]. AQWA© uses a potential theory based panel method to estimate the roll damping due to the wave making.

The wave making component accounts for between 5% and 30% of the roll damping for a general-cargo type ship. However, the component may have a larger effect for ships with a shallow draught and wide sections [79].

In order to compare the accuracy of roll wave damping predictions by AQWA©, rectangular and circular cylinders for which experimental roll damping measurements are provided by Vugts [3] are considered. The dimensions of the rectangular and circular cylinders are presented in the following Table 4.1.

Table 4.1 : The dimensions of the rectangular and circular cylinders.

Specifications	Dimensions	Rectangular Cylinder	Circular Cylinder
Length	L (m)	25	50
Breadth	B (m)	5	10
Draft	T (m)	2.5	5
Sectional wetted surface area	A (m^2)	12.5	39.27

Figures 4.1 and 4.2 presents the panel models of rectangular and cylindrical shapes

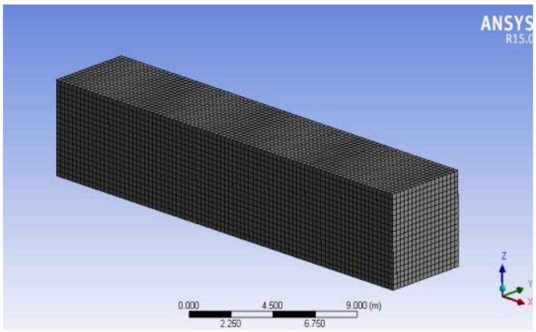

Figure 4.1 : The panel model of rectangular shaped floating body.

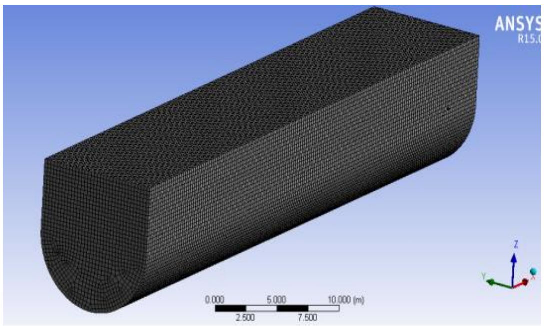

Figure 4.2 : The panel model of cylindrical shaped floating body.

Table 4.2 presents Comparison of Vugts' rectangular section roll damping experiments and AQWA© Results. The results of cylindrical shapes are zero for Frank-Close-Fit and AQWA© since cylindrical shapes are highly affected by viscous effects and Frank-Close-Fit and AQWA© calculates wave making component without viscous effects. To take viscous effects into account, see Chapter 5.

Frank Close-Fit predictions are based on calculations performed by Vugts [3]. The curves are digitized by GetData©.

Table 4.2 : Comparison of Vugts' rectangular section roll damping experiments and AQWA© Results.

Experiment [3]		**Frank Close-Fit** [3]		**AQWA©**			
$\omega\sqrt{\frac{B}{2g}}$	$\frac{b_{44}}{\rho AB^2}\sqrt{\frac{B}{2g}}$	$\omega\sqrt{\frac{B}{2g}}$	$\frac{b_{44}}{\rho AB^2}\sqrt{\frac{B}{2g}}$	$\omega\sqrt{\frac{B}{2g}}$	ω	B_{44}	$\frac{b_{44}}{\rho AB^2}\sqrt{\frac{B}{2g}}$
0.22	0.0001	0.22	0	0.05	0.10	0.00	0.0000
0.29	0.0003	0.29	0	0.15	0.30	0.01	0.0000
0.36	0.003	0.36	0.0019	0.25	0.49	0.34	0.0000
0.43	0.0068	0.43	0.0031	0.35	0.69	3.76	0.0002
0.5	0.01	0.5	0.0065	0.45	0.89	23.35	0.0015
0.57	0.015	0.57	0.011	0.55	1.08	94.09	0.0059
0.65	0.018	0.65	0.014	0.65	1.28	226.99	0.0143
0.72	0.02	0.72	0.017	0.75	1.48	318.14	0.0200
0.79	0.021	0.79	0.0185	0.84	1.68	328.10	0.0206
0.86	0.0209	0.86	0.0188	0.94	1.87	324.83	0.0204
0.93	0.0212	0.93	0.0188	1.04	2.07	305.75	0.0192
1	0.02	1	0.0173	1.14	2.27	267.41	0.0168
1.14	0.0197	1.14	0.016	1.24	2.46	243.57	0.0153
1.21	0.0188	1.21	0.0145	1.34	2.66	212.07	0.0133
1.28	0.0182	1.28	0.013	1.44	2.86	178.34	0.0112
1.35	0.0176	1.35	0.0121	1.54	3.05	149.74	0.0094
1.43	0.017	1.43	0.0106	1.64	3.25	120.80	0.0076
1.57	0.0164	1.57	0.009	1.74	3.45	98.65	0.0062
1.71	0.0149	1.71	0.007	1.84	3.64	78.70	0.0050

Figure 4.3 illustrates that rectangular structures are predominantly influenced by radiation damping, with AQWA© effectively calculating the wave-making (radiation) component of roll damping to a satisfactory extent. Conversely, Figure 4.4 demonstrates that cylindrical structures are significantly impacted by other viscous

effects compared to rectangular shapes. Additionally, in Figure 4.4, it is evident that vessels or ship-like cross sections are notably affected by other viscous effects rather than radiation damping. It can briefly seen that AQWA© does not consider skin friction component of Ikeda roll damping method, thus it will be calculated empirically and added to program. Non-dimensional roll RAO for rectangular structure is shown in Figure 4.3.

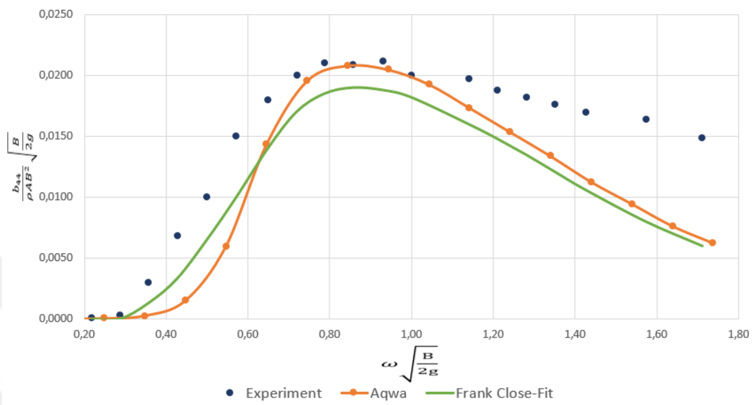

Figure 4.3 : Comparison of Vugts' body roll damping of rectangular section.

Non dimensional roll RAO for semi-cylindrical structure is shown in Figure 4.4.

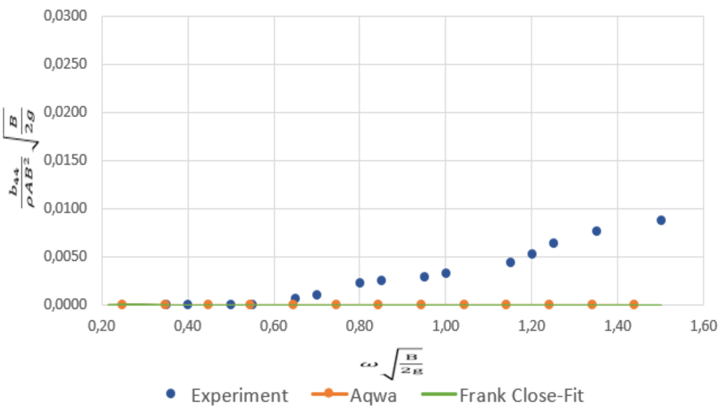

Figure 4.4 : Comparison of Vugts' body roll damping of semi-cylindrical section.

Wave damping is a function of forward velocity and wave frequency. The presence of forward velocity changes wave damping.

Ikeda [80] recommends a formulation for predicting the forward speed wave damping from the zero speed radiation wave damping. However, strip theory based methods [76] are proven to be sufficiently accurate to predict the forward speed radiation damping and should be used instead of the empirical formulae specified by Ikeda [18]. In this study, AQWA© will be used to calculate wave damping. AQWA© exclusively computes the wave-making component of roll damping ,while other viscous effects are not included in the program and must be incorporated separately for consideration in motion analysis.

5. IKEDA METHOD FOR ESTIMATING VISCOUS ROLL DAMPING

This chapter provides a detailed explanation of the practical roll damping prediction model proposed by Japanese researcher Ikeda [79],which has been widely adopted as the prevailing industry norm for predicting the roll damping of ship-shaped vessels. The equivalent linear damping B_{eq} is assumed to be divided into 4 components as skin friction damping B_F , eddy damping B_E , lift damping B_L and bilge keel damping B_{BK} as follows:

$$B_{eq} = B_F + B_L + B_E + B_{BK} \tag{5.1}$$

5.1. Skin Friction Damping

This component is influenced by Reynolds number (scale effects), and so the proportion decreases in proportion to ship size and only accounts for between 1% and 3% for full scale ships. Other components of the roll damping do not have such scale effects. Therefore, even if the scale of a ship is varied, the same non-dimensional damping coefficient can be used for the other components excluding the frictional component. [79]

Skin friction drag occurs due to the frictional resistance exerted by the viscous stress on the surface of the hull. Kato (1958) proposed an empirical formula for calculating the skin friction damping coefficient in laminar flow, as presented in Equation 5.2.

$$B_{f0} = \frac{4}{3\pi}\rho S {r_e}^3 R_0 \omega C_f \tag{5.2}$$

$$C_f = 1.328\sqrt{\frac{2\pi v}{3.22 {r_e}^2 R_0^2 \omega}} \tag{5.3}$$

$$r_e = \frac{1}{\pi}\left[(0.887 + 0.145 C_B)\frac{S}{L} - 2OG\right] \tag{5.4}$$

Where

ρ : the density of the fluid

r_e : the effective bilge radius

R_0: the roll amplitude

ω : the frequency of excitation

C_f : the friction coefficient

v : the kinematic viscosity of fluid

C_B : the block coefficient of the ship

L : the length of the ship

B : the breadth of the ship

T : the draft of the ship

OG : the distance between the roll center of the ship and the center of gravity

S : the wetted surface area which is empirically calculated as follows:

$$S = L(1.7T + C_B B) \tag{5.5}$$

While the model operates under laminar flow conditions due to its size, the actual ship at full scale encounters turbulent flow. Therefore, Equation 5.2 needs adjustment to accommodate turbulent flow, as outlined in Equation 5.6. The second term in Equation 5.6 represents the correction factor necessary to address turbulent flow effects.

$$B_{f0} = 0.787\rho S r_e^2 \sqrt{v\omega}\left\{1 + 0.00814\left(\frac{r_e^2 R_0^2 \omega}{v}\right)^{0.386}\right\} \tag{5.6}$$

Schmitke (1978) provides modification in equation 5.7 for a ship moving with forward speed U.

$$B_F = B_{f0}\left(1 + 4.1\frac{U}{\omega L}\right) \tag{5.7}$$

To apply this component in AQWA©, details are given in next section of this chapter.

5.2. Lift Damping

Since the lift force acts on the ship hull moving forward with sway motion, it can therefore be concluded that a lift effect occurs for ships during roll motion as well. Ikeda (1978) provide a simple empirical formulation for calculating the lift component of the roll damping as shown in equation 3.16. C_M represents the mid-ship cross section coefficient.

$$B_L = 0.075\rho ULT^3 k_N \left[1 - 2.8\frac{OG}{T} + 4.667\left(\frac{OG}{T}\right)^2\right] \quad (5.8)$$

$$k_N = 2\pi\frac{T}{L} + \kappa\left(4.1\frac{B}{L} - 0.045\right)$$

$$\kappa = 0 \text{ for } C_M \leq 0.92$$

$$\kappa = 0.1 \text{ for } \quad 0.92 \leq C_M \leq 0.97$$

$$\kappa = 0.3 \text{ for } \quad 0.97 \leq C_M \leq 0.99$$

It can be observed from the formula presented in equation 3.16 that the lift damping coefficient changes proportionally with the speed U and unaffected by the frequency of roll motion. In this thesis, lift damping will be calculated empirically by Equation 5.8.

5.3. Eddy Damping and Bilge Keel Damping

At zero forward speed, the eddy making component for a naked hull is mainly due to the sectional vortices. Figure 5.1 shows a ship-like cross section where the bilge damping is taken into account. To check whether eddy from the bilge is occurring, the relative flow velocity at bilge and the roll natural frequency of the vessel are calculated. To do so, the Keulegan-Carpenter number at each time step is used, which is defined as

$$K_{cb} = \frac{R_b|\dot{\varphi}|T_R}{2r_B} \quad (5.9)$$

Where R_b is the distance from roll center to bilge tangent, r_B is the bilge Radius, $\dot{\varphi}$ is the relative angular roll velocity to the wave slope, T_R is the roll period at resonance.

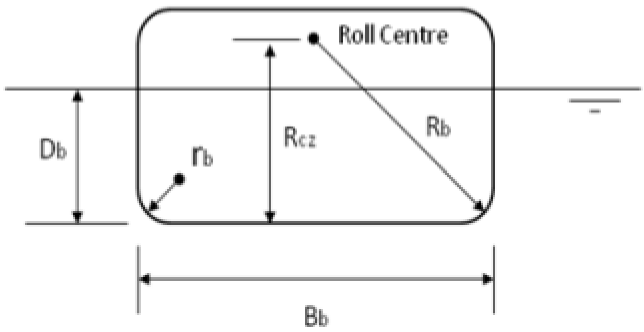

Figure 5.1 : Ship-like cross section with bilge [76].

It is assumed that eddy damping is null if $K_{cb} < 10$. Otherwise the roll moment due to bilge vortex shedding induced nonlinear damping at each time step is calculated by

$$M_{roll} = \frac{1}{2}\rho C_{db} {B_b}^4 L_b |\dot{\varphi}| \dot{\varphi} \tag{5.10}$$

Where L_b is the bilge length and C_{db} is a non-dimensional roll damping coefficient. The non-dimensional roll damping coefficient C_{db} is interpolated from a database, which is a function of bilge geometric properties:

$$C_{db} = C_{db}\left(\frac{B_b}{D_b}, \frac{R_{cz}}{D_b}\right) \tag{5.11}$$

Where B_b and C_{db} are the breadth and draft of cross section and R_{cz} is the distance between the cross sectional baseline and the roll center.

5.4. Critical Damping Method

In chapter 1, it is presented that Park et al. [21] conducted experiments and numerical simulations to estimate the added resistance of a large tanker in oblique waves. In his study, the results calculated by panel method showed good agreement with the experimental results. Notably, viscous roll damping was considered in the calculations by taking 3% of the critical roll damping. (the 3% is obtained through fitting with free roll decay test of the SSPA experiment).

This part aims to explore the explanation of the critical roll damping approach with the Ikeda method to enhance understanding. The critical damping method encompasses the fundamental aspects of the Ikeda method, particularly focusing on accounting for viscous effects. AQWA© software enables the computation of the wave-making, bilge keel, and Eddy components which are components of the Ikeda method. Therefore, this chapter efforts to employ the critical damping method to evaluate the skin friction damping component of the Ikeda method.

The practice of including a linearized viscous damping component is widespread, particularly in addressing the pronounced non-linearity of damping forces, notably evident in roll motion. This additional term is typically simplified as a fraction of critical damping for ease of calculation [82-86].

$$([M + A(\omega)]\ddot{\varphi} + [B_{44T}]\dot{\varphi} + [C]\varphi) = 0 \tag{5.12}$$

This equation can be written in a more standard form by dividing by the $[\mathrm{M}+\mathrm{A}(\omega)]$:

$$\ddot{\varphi} + 2\mathrm{v}\dot{\varphi} + {\omega_0}^2\,\varphi = 0 \tag{5.13}$$

$$\mathrm{v} \equiv \frac{\mathrm{B_{44T}}}{2(\mathrm{M}+\mathrm{A}(\omega))}\ ;\ \omega_0 \equiv \sqrt{\frac{\mathrm{C}}{\mathrm{M}+\mathrm{A}(\omega)}} \tag{5.14}$$

It should be recalled that the solution of equation 5.13 is of the form

$$\varphi(\mathrm{t}) = \ \varphi_0 e^{\sigma t} \tag{5.15}$$

where φ_0 is the initial roll amplitude. Substituing equation 5.15 in equation 5.13 yields the auxiliary equation.

$$\sigma^2 + 2\mathrm{v}\sigma + {\omega_0}^2\ = 0 \tag{5.16}$$

Solving for σ we obtain

$$\sigma = -\mathrm{v} \pm \sqrt{\mathrm{v}^2 - \omega_0^2} \tag{5.17}$$

If $v = \omega_0$, is known as "critically damped" , in this case equation 5.14 gives

$$\mathrm{B_{44T}} = \mathrm{nB_{cr}} = \mathrm{n}2\sqrt{(\mathrm{M}+\mathrm{A}(\omega))\mathrm{C}} \tag{5.18}$$

If

$$\frac{\mathrm{B_{44T}}}{\mathrm{B_{cr}}} = \mathrm{n} = 1 \tag{5.19}$$

Then the system is critically damped. Thus:

$$\mathrm{B_{44T}} = \mathrm{B_{cr}} = 2\sqrt{(\mathrm{M}+\mathrm{A}(\omega))\mathrm{C}} \tag{5.20}$$

M: mass matrix

$$\begin{bmatrix} \mathrm{m} & 0 & 0 & 0 & 0 & 0 \\ 0 & \mathrm{m} & 0 & 0 & 0 & 0 \\ 0 & 0 & \mathrm{m} & 0 & 0 & 0 \\ 0 & 0 & 0 & \mathrm{I_x} & 0 & 0 \\ 0 & 0 & 0 & 0 & \mathrm{I_y} & 0 \\ 0 & 0 & 0 & 0 & 0 & \mathrm{I_z} \end{bmatrix}$$

where m is mass of the ship.

A: added mass matrix

$$\begin{bmatrix} A_{11} & A_{12} & A_{13} & A_{14} & A_{15} & A_{16} \\ A_{21} & A_{22} & A_{23} & A_{24} & A_{25} & A_{26} \\ A_{31} & A_{32} & A_{33} & A_{34} & A_{35} & A_{36} \\ A_{41} & A_{42} & A_{43} & A_{44} & A_{45} & A_{46} \\ A_{51} & A_{52} & A_{53} & A_{54} & A_{55} & A_{56} \\ A_{61} & A_{62} & A_{63} & A_{64} & A_{65} & A_{66} \end{bmatrix}$$

C: Hydrostatic restoring force matrix

$$\begin{bmatrix} 0 & 0 & 0 & 0 & 0 & 0 \\ 0 & 0 & 0 & 0 & 0 & 0 \\ 0 & 0 & C_{33} & C_{34} & C_{35} & 0 \\ 0 & 0 & C_{43} & C_{44} & C_{45} & C_{46} \\ 0 & 0 & C_{53} & C_{54} & C_{55} & C_{56} \\ 0 & 0 & 0 & 0 & 0 & 0 \end{bmatrix}$$

Mass matrix, added mass matrix and hydrostatic restoring force matrices are the outcome of AQWA©.

After this method is being applied, roll motion of the structure will be critically damped in time domain as presented in Figure 5.2.

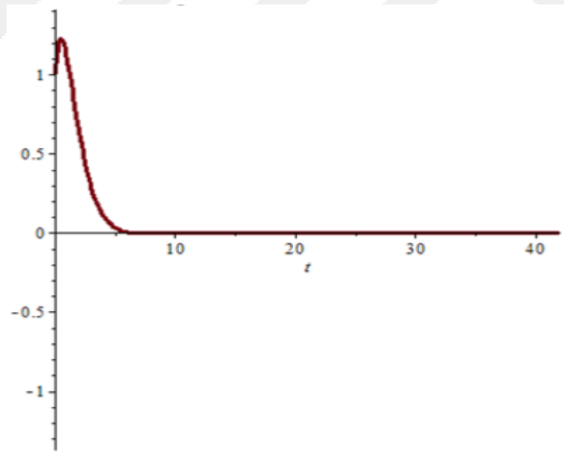

Figure 5.2 : Generic critical damping angular roll motion versus time [20].

Skin friction will be accounted by incorporating the decay test outcomes of the structure under examination for roll motion analysis. The damping property for a specified degree of freedom of a floating structure can be estimated using a numerical twang test record. As shown in Figure 5.3, the structure center of gravity is shifted by a distance ΔX along the specified degree of freedom from its equilibrium position in still water at time. A time history of its freely-decaying response can then be calculated by an AQWA© time domain analysis.

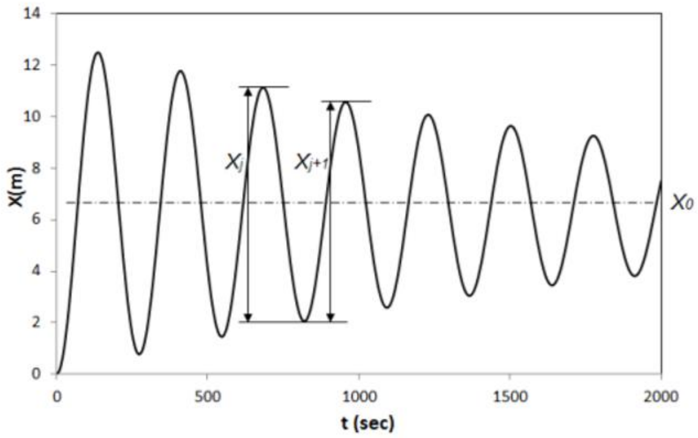

Figure 5.3 : Generic freely-decaying record [81].

Assuming that the motion in this degree of freedom has no interaction with other motions, and that there are no other external dynamic forces, the linear single degree of freedom dynamic system has an analytical response of the form [81]:

$$X(t) = X_0 + \Delta X e^{-\zeta_c \omega_n t} \cos(\omega_d t) \tag{5.21}$$

where ω_n is the natural frequency,

$$\omega_d = \omega_n \sqrt{1 - \zeta_c^2} \tag{5.22}$$

is the damped natural frequency, and ζ_c is the required percentage of critical damping. The percentage of critical damping may be measured by the logarithmic decrement

$$d_c = \ln\left(\frac{X_j^{max} - X_0}{X_{j+1}^{max} - X_0}\right) = \frac{2\pi\zeta_c}{\sqrt{1 - {\zeta_c}^2}} \tag{5.23}$$

where X_j^{max} and X_{j+1}^{max} are the heights of two successive maxima. Based on the linear dynamic system assumption, the ratio of the heights of two successive maxima is approximately equal to the square of the ratio of the heights of a crest-trough and its adjacent troughcrest, such as X_j and X_{j+1} shown in Figure 5.3. The linear percentage of critical damping can therefore be estimated by

$$\zeta_{cj} = \frac{d_c}{\sqrt{{d_c}^2 + 4\pi^2}} \tag{5.24}$$

Where

$$d_c = \ln\left(\frac{X_j^{max} - X_0}{X_{j+1}^{max} - X_0}\right) = 2\ln\left(\frac{X_j}{X_{j+1}}\right) \quad (5.25)$$

Let the linear percentage of the structure is “a”, then viscous roll damping of the structure will be %a of the critical roll damping as shown in Figure 5.4. By using equation 5.20, we can have the equation 5.26 below:

$$B_v = \frac{a2\sqrt{(M + A(\omega)C}}{100} \quad (5.26)$$

To obtain the critical damping value of DTMB 5415 hull model, experimental roll decay graphic at the angle of 15 degrees of DTMB 5415 model is used [83].

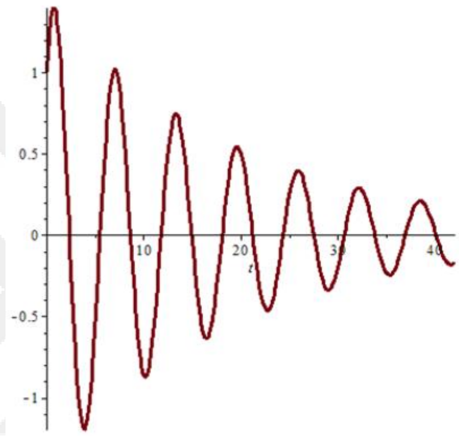

Figure 5.4 : %a of the critical damping angular roll motion versus time [20].

6. EFFECT OF BILGE KEEL DIMENSIONS ON ROLL MOTION

6. 1. Validation of Bare Hull DTMB 5415 Hull

In this chapter, a validation study for bare hull DTMB 5415 warship model is presented.

Specifications of the model presented in Table 6.1.

Table 6.1 : Main particulars of US navy destroyer hull 5415 [84].

Particulars	Model(1/51)
L_{OA} (m)	3
L_{PP} (m)	2.788
B_{WL} (m)	0.374
B_{OA} (m)	0.403
D (m)	0.244
T (m)	0.120
V (m)	0.0635
$\Delta(m^3)$	0.063
C_B	0.505
C_P	0.616
C_M	0.815
KM (m)	0.186
KG (m)	0.148
GM (m)	0.038
LCG (m)	1.375
kxx (m)	0.136
kyy (m)	0.696
kzz (m)	0.696

Begovic [84] provided a detailed analysis of the motion predictions for the DTMB 5415 hull under both intact and damaged conditions, utilizing experimental data from 1/51 scale. These experiments are conducted at zero speed in head, beam, and quartering seas. The findings for the 1/51 model are expressed through RAOs. Intact ship data obtained by this study roll non-dimensional values of 5415 with the wave angle 90^o presented below in Table 6.2.

Table 6.2 : Roll non-dimensional values obtained by experiment [84].

ω (rad/s)	$\omega\sqrt{\frac{L}{g}}$	η_{44}/kA
2.712	1.5	1.183
2.816	1.557	1.553
3.056	1.69	1.627
3.291	1.82	1.750
3.588	1.984	2.511
3.882	2.147	3.393
4.061	2.246	4.768
4.266	2.359	7.235
4.530	2.505	5.406
4.765	2.635	2.624
5.356	2.962	1.272

5415 model ship is studied in AQWA© according to specifications in Table 6.1. Model of the ship presented in Figure 6.1.

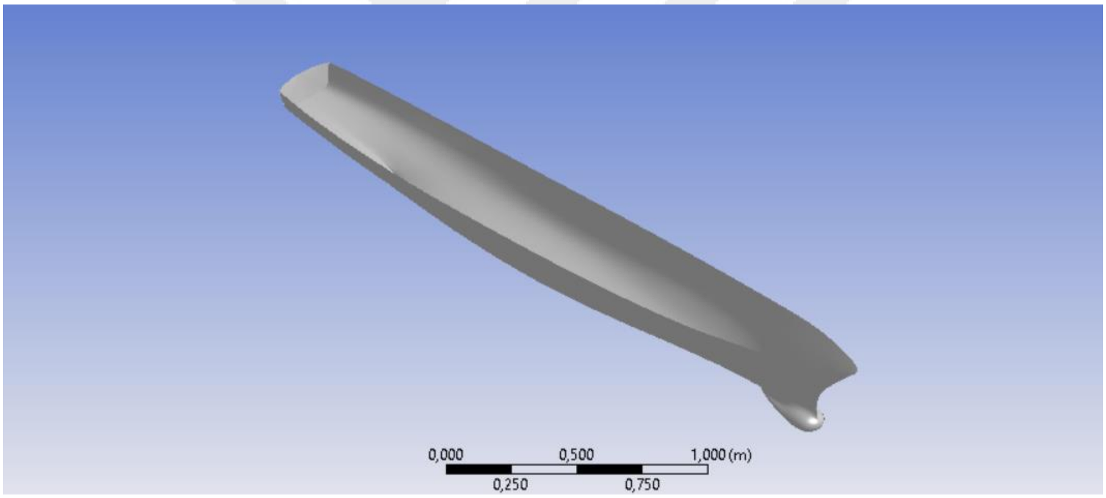

Figure 6.1 : DTMB 5415 Model.

For obtaining the correct roll non-dimensional values by AQWA©, Empirical Ikeda Method (see detailed in Chapter 5) is applied. Results of AQWA© presented in Table 6.3.

Table 6.3 : Roll non-dimensional values obtained by AQWA©.

ω (rad/s)	$\omega\sqrt{\frac{L}{g}}$	η_{44}/kA
2.675	1.479	0.316
2.836	1.568	0.381
2.997	1.657	0.462
3.158	1.746	0.566
3.319	1.835	0.704
3.480	1.924	0.895
3.641	2.013	1.180
3.802	2.103	1.647
3.963	2.192	2.542
4.124	2.281	4.698
4.285	2.370	7.321
4.446	2.459	4.109
4.607	2.548	2.530
4.768	2.637	1.819
4.920	2.721	1.424
5.090	2.815	1.174
5.251	2.904	1.001
5.412	2.993	0.873

Comparison of experimental and simulated non-dimensional roll values shown in Figure 6.2.

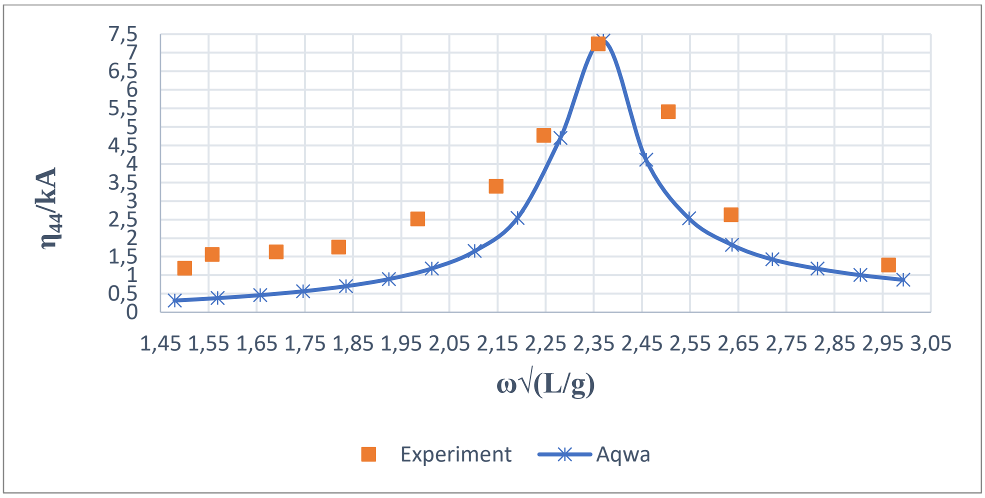

Figure 6.2 : Comparison of experiment and AQWA© non-dimensional roll of DTMB 5415.

6.2. Parametric Analyses of DTMB 5415 Hull

To evaluate the effect of bilge keels on roll motion, six different type of bilge keels are studied. Since there is lots of parametric analysis, to be able to follow the analyses properly, each bilge keel dimensions are explained and numbered below in Table 6.4.

Table 6.4 : Dimensions of bilge keels [85].

<table>
<tr>
<td>BK060
L_{BK}=927,5 mm
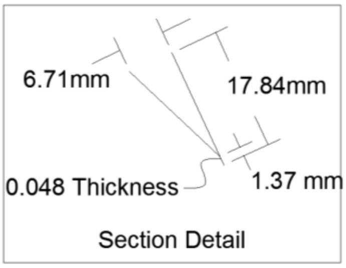
</td>
<td>BK160
L_{BK}=1159,15 mm
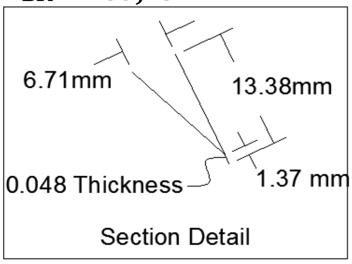
</td>
<td>BK260
L_{BK}=927,5 mm
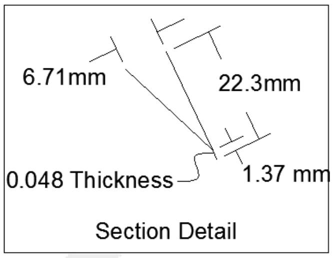
</td>
</tr>
<tr>
<td>BK030
L_{BK}=927,5 mm
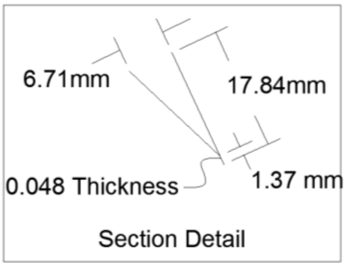
</td>
<td>BK130
L_{BK}=1159,15 mm
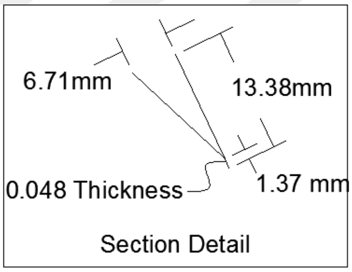
</td>
<td>BK230
L_{BK}=927,5 mm
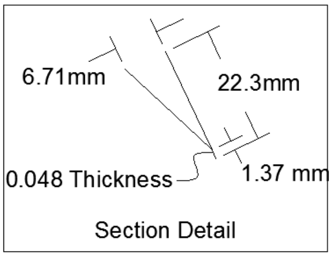
</td>
</tr>
</table>

In Table 6.4, BK is Bilge Keel; 0, 1 and 2 are the types of bilge keels according to width of the bilge keel and 30, 60 are the angles of bilge keels mounted to hull. L_{BK} is the length of bilge keel. BK060 represents the original bilge keel of 5415 ship. The dimensions of the bilge keels created by increasing and/or decreasing the length and width of the original bilge keel by %25 by considering the limitations explained in Chapter 2, Section 2.1.1.

Table 6.5 presents the η_{44}/kA non-dimensional roll values of DTMB 5415 model mounted BK060 bilge keel model.

Table 6.5 : BK060 bilge keel non-dimensional roll η_{44}/kA values.

BK060, Fn=0			BK060, Fn=0,15			BK060, Fn=0,30		
ω (rad/s)	$\omega\sqrt{\frac{L}{g}}$	η_{44}/kA	ω (rad/s)	$\omega\sqrt{\frac{L}{g}}$	η_{44}/kA	ω (rad/s)	$\omega\sqrt{\frac{L}{g}}$	η_{44}/kA
2.602	1.439	0.301	2.602	1.439	0.311	2.602	1.439	0.332
2.781	1.538	0.373	2.781	1.538	0.386	2.781	1.538	0.410
2.959	1.636	0.466	2.959	1.636	0.482	2.959	1.636	0.512
3.138	1.735	0.591	3.138	1.735	0.611	3.138	1.735	0.649
3.317	1.834	0.766	3.317	1.834	0.793	3.317	1.834	0.843
3.495	1.933	1.031	3.495	1.933	1.068	3.495	1.933	1.137
3.674	2.032	1.480	3.674	2.032	1.533	3.674	2.032	1.630
3.853	2.131	2.391	3.853	2.131	2.462	3.853	2.131	2.598
4.032	2.229	4.864	4.032	2.229	4.768	4.032	2.229	4.796
4.210	2.328	6.593	4.210	2.328	6.093	4.210	2.328	5.761
4.389	2.427	3.281	4.389	2.427	3.343	4.389	2.427	3.415
4.568	2.526	2.059	4.568	2.526	2.156	4.568	2.526	2.264
4.746	2.625	1.504	4.746	2.625	1.595	4.746	2.625	1.695
4.925	2.724	1.191	4.925	2.724	1.273	4.925	2.724	1.361
5.104	2.822	0.990	5.104	2.822	1.063	5.104	2.822	1.142
5.282	2.921	0.848	5.282	2.921	0.915	5.282	2.921	0.986
5.461	3.020	0.742	5.461	3.020	0.804	5.461	3.020	0.867
5.640	3.119	0.659	5.640	3.119	0.716	5.640	3.119	0.774

The values in Table 6.5 are presented as graphics in Figure 6.3.

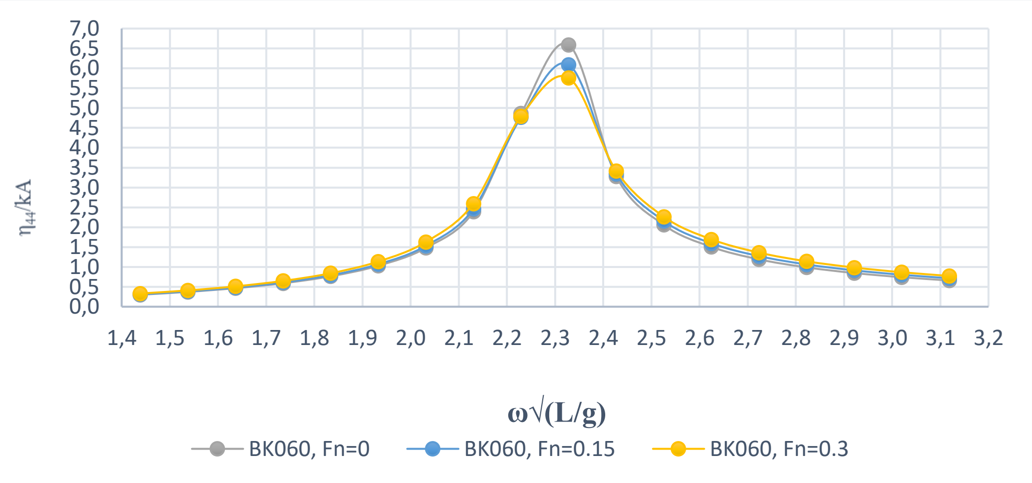

Figure 6.3 : BK060 bilge keel non-dimensional roll η_{44}/kA graphics.

Table 6.6 presents the η_{44}/kA values of DTMB 5415 model mounted BK160 bilge keel model.

Table 6.6 : BK160 bilge keel non-dimensional roll η_{44}/kA values.

BK160, Fn=0			BK160, Fn=0,15			BK160, Fn=0,30		
ω (rad/s)	$\omega\sqrt{\frac{L}{g}}$	η_{44}/kA	ω (rad/s)	$\omega\sqrt{\frac{L}{g}}$	η_{44}/kA	ω (rad/s)	$\omega\sqrt{\frac{L}{g}}$	η_{44}/kA
2.459	1.360	0.257	2.459	1.360	0.263	2.459	1.360	0.275
2.640	1.460	0.319	2.640	1.460	0.326	2.640	1.460	0.341
2.821	1.560	0.397	2.821	1.560	0.407	2.821	1.560	0.425
3.003	1.661	0.501	3.003	1.661	0.512	3.003	1.661	0.535
3.184	1.761	0.642	3.184	1.761	0.657	3.184	1.761	0.686
3.366	1.861	0.846	3.366	1.861	0.866	3.366	1.861	0.905
3.547	1.962	1.169	3.547	1.962	1.198	3.547	1.962	1.250
3.729	2.062	1.758	3.729	2.062	1.795	3.729	2.062	1.866
3.910	2.162	3.111	3.910	2.162	3.112	3.910	2.162	3.169
4.091	2.263	6.734	4.091	2.263	5.999	4.091	2.263	5.530
4.273	2.363	4.586	4.273	2.363	4.397	4.273	2.363	4.221
4.454	2.463	2.513	4.454	2.463	2.556	4.454	2.463	2.592
4.636	2.564	1.714	4.636	2.564	1.776	4.636	2.564	1.836
4.817	2.664	1.307	4.817	2.664	1.367	4.817	2.664	1.428
4.999	2.764	1.061	4.999	2.764	1.118	4.999	2.764	1.174
5.180	2.865	0.895	5.180	2.865	0.948	5.180	2.865	1.000
5.361	2.965	0.775	5.361	2.965	0.824	5.361	2.965	0.873
5.543	3.065	0.683	5.543	3.065	0.729	5.543	3.065	0.774

The values in Table 6.6 are presented as graphics in Figure 6.4.

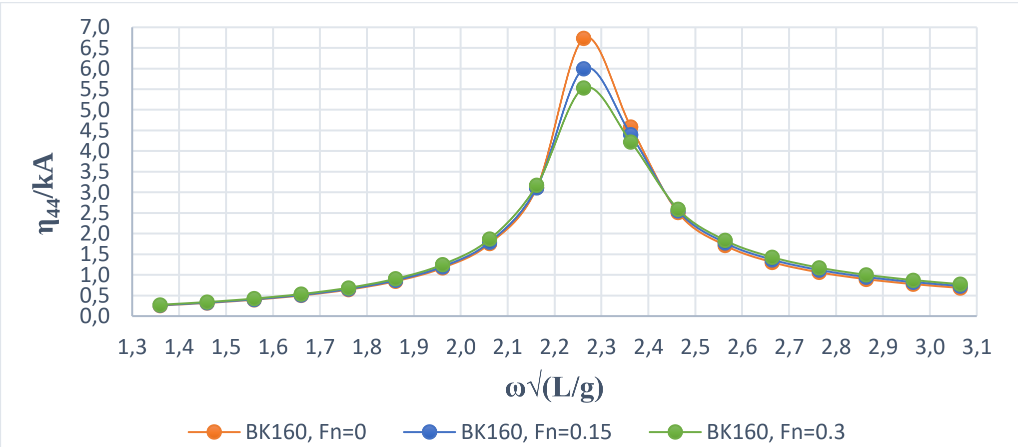

Figure 6.4 : BK160 bilge keel non-dimensional roll η_{44}/kA graphics.

Table 6.7 presents the η_{44}/kA values of DTMB 5415 model mounted BK260 bilge keel model.

Table 6.7 : BK260 bilge keel non-dimensional roll η_{44}/kA values.

BK260, Fn=0			BK260, Fn=0,15			BK260, Fn=0,30		
ω (rad/s)	$\omega\sqrt{\frac{L}{g}}$	η_{44}/kA	ω (rad/s)	$\omega\sqrt{\frac{L}{g}}$	η_{44}/kA	ω (rad/s)	$\omega\sqrt{\frac{L}{g}}$	η_{44}/kA
2.593	1.434	0.300	2.593	1.434	0.310	2.593	1.434	0.329
2.771	1.532	0.373	2.771	1.532	0.384	2.771	1.532	0.407
2.949	1.631	0.467	2.949	1.631	0.481	2.949	1.631	0.510
3.127	1.729	0.592	3.127	1.729	0.611	3.127	1.729	0.648
3.305	1.828	0.770	3.305	1.828	0.796	3.305	1.828	0.844
3.483	1.926	1.042	3.483	1.926	1.078	3.483	1.926	1.143
3.661	2.025	1.508	3.661	2.025	1.560	3.661	2.025	1.653
3.839	2.123	2.476	3.839	2.123	2.541	3.839	2.123	2.669
4.017	2.222	5.174	4.017	2.222	5.009	4.017	2.222	4.975
4.195	2.320	6.195	4.195	2.320	5.777	4.195	2.320	5.483
4.373	2.418	3.089	4.373	2.418	3.154	4.373	2.418	3.227
4.551	2.517	1.971	4.551	2.517	2.064	4.551	2.517	2.166
4.729	2.615	1.454	4.729	2.615	1.540	4.729	2.615	1.634
4.907	2.714	1.158	4.907	2.714	1.236	4.907	2.714	1.320
5.086	2.812	0.965	5.086	2.812	1.036	5.086	2.812	1.111
5.264	2.911	0.829	5.264	2.911	0.894	5.264	2.911	0.962
5.442	3.009	0.727	5.442	3.009	0.787	5.442	3.009	0.848
5.620	3.108	0.648	5.620	3.108	0.703	5.620	3.108	0.758

The values in Table 6.7 are presented as graphics in Figure 6.5.

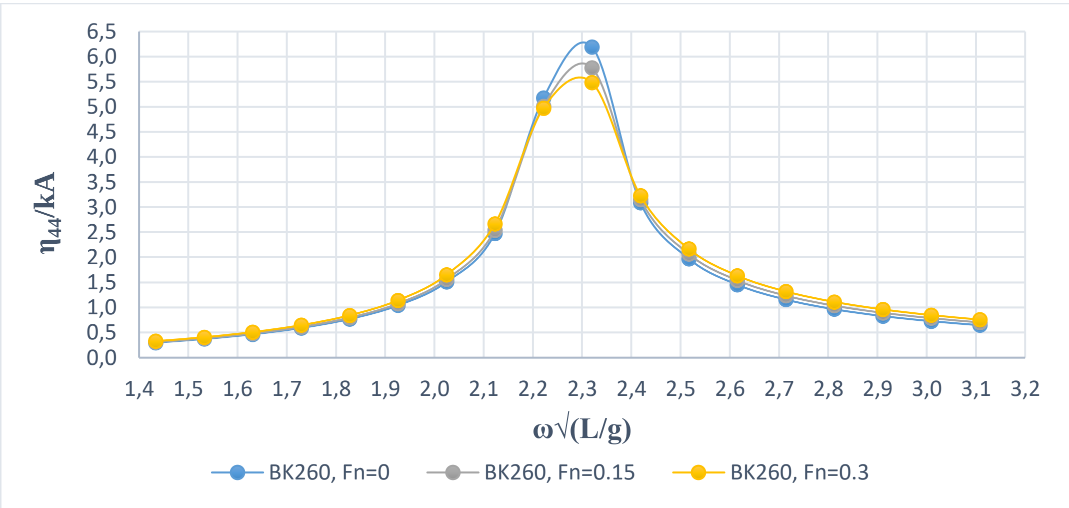

Figure 6.5 : BK260 bilge keel non-dimensional roll η_{44}/kA graphics.

Table 6.8 presents the η_{44}/kA values of DTMB 5415 model mounted BK030 bilge keel model.

Table 6.8 : BK030 bilge keel non-dimensional roll η_{44}/kA values.

BK030, Fn=0			BK030, Fn=0,15			BK030, Fn=0,30		
ω (rad/s)	$\omega\sqrt{\frac{L}{g}}$	η_{44}/kA	ω (rad/s)	$\omega\sqrt{\frac{L}{g}}$	η_{44}/kA	ω (rad/s)	$\omega\sqrt{\frac{L}{g}}$	η_{44}/kA
2.642	1.461	0.316	2.642	1.461	0.327	2.642	1.461	0.349
2.812	1.555	0.388	2.812	1.555	0.402	2.812	1.555	0.428
2.981	1.649	0.481	2.981	1.649	0.497	2.981	1.649	0.530
3.151	1.742	0.604	3.151	1.742	0.625	3.151	1.742	0.666
3.320	1.836	0.775	3.320	1.836	0.804	3.320	1.836	0.856
3.490	1.930	1.032	3.490	1.930	1.070	3.490	1.930	1.141
3.659	2.023	1.456	3.659	2.023	1.511	3.659	2.023	1.609
3.829	2.117	2.286	3.829	2.117	2.358	3.829	2.117	2.494
3.998	2.211	4.396	3.998	2.211	4.358	3.998	2.211	4.429
4.168	2.305	7.047	4.168	2.305	6.395	4.168	2.305	5.981
4.337	2.398	3.672	4.337	2.398	3.704	4.337	2.398	3.747
4.507	2.492	2.244	4.507	2.492	2.342	4.507	2.492	2.451
4.676	2.586	1.615	4.676	2.586	1.709	4.676	2.586	1.814
4.845	2.680	1.268	4.845	2.680	1.353	4.845	2.680	1.446
5.015	2.773	1.047	5.015	2.773	1.125	5.015	2.773	1.208
5.184	2.867	0.894	5.184	2.867	0.965	5.184	2.867	1.040
5.354	2.961	0.781	5.354	2.961	0.846	5.354	2.961	0.913
5.523	3.054	0.693	5.523	3.054	0.753	5.523	3.054	0.814

The values in Table 6.8 are presented as graphics in Figure 6.6.

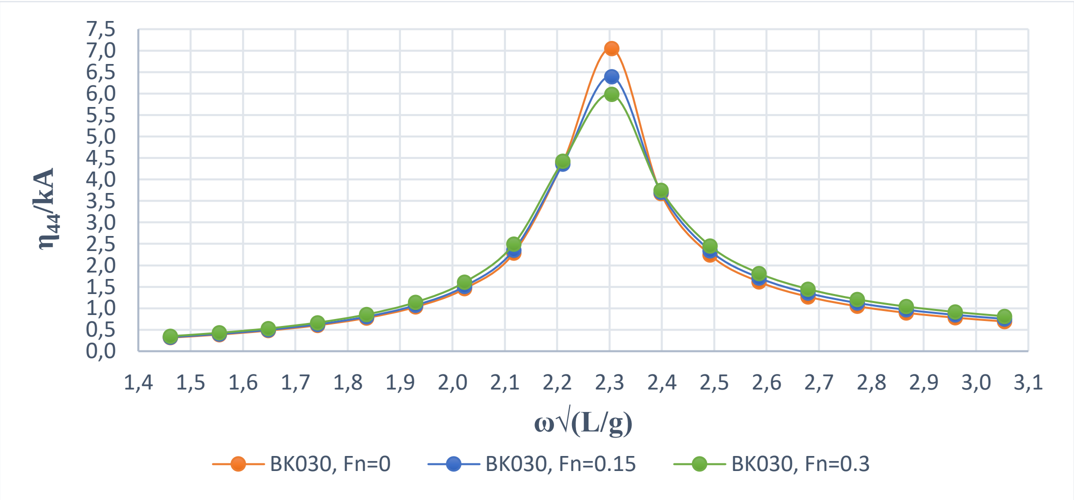

Figure 6.6 : BK030 bilge keel non-dimensional roll η_{44}/kA graphics.

Table 6.9 presents the η_{44}/kA values of DTMB 5415 model mounted BK130 bilge keel model.

Table 6.9 : BK130 bilge keel non-dimensional roll η_{44}/kA values.

BK130, Fn=0			BK130, Fn=0,15			BK130, Fn=0,30		
ω (rad/s)	$\omega\sqrt{\frac{L}{g}}$	η_{44}/kA	ω (rad/s)	$\omega\sqrt{\frac{L}{g}}$	η_{44}/kA	ω (rad/s)	$\omega\sqrt{\frac{L}{g}}$	η_{44}/kA
2.658	1.470	0.324	2.658	1.470	0.332	2.658	1.470	0.350
2.840	1.571	0.406	2.840	1.571	0.416	2.840	1.571	0.437
3.023	1.672	0.514	3.023	1.672	0.527	3.023	1.672	0.553
3.206	1.773	0.664	3.206	1.773	0.681	3.206	1.773	0.714
3.388	1.874	0.888	3.388	1.874	0.910	3.388	1.874	0.954
3.571	1.975	1.258	3.571	1.975	1.287	3.571	1.975	1.346
3.754	2.076	1.979	3.754	2.076	2.006	3.754	2.076	2.078
3.936	2.177	3.845	3.936	2.177	3.702	3.936	2.177	3.651
4.119	2.278	6.554	4.119	2.278	5.592	4.119	2.278	5.000
4.302	2.379	3.307	4.302	2.379	3.252	4.302	2.379	3.201
4.485	2.480	1.991	4.485	2.480	2.041	4.485	2.480	2.094
4.667	2.581	1.424	4.667	2.581	1.482	4.667	2.581	1.545
4.850	2.682	1.114	4.850	2.682	1.169	4.850	2.682	1.230
5.033	2.783	0.917	5.033	2.783	0.969	5.033	2.783	1.025
5.215	2.884	0.781	5.215	2.884	0.829	5.215	2.884	0.881
5.398	2.985	0.680	5.398	2.985	0.726	5.398	2.985	0.773
5.581	3.086	0.602	5.581	3.086	0.645	5.581	3.086	0.689
5.763	3.187	0.539	5.763	3.187	0.580	5.763	3.187	0.621

The values in Table 6.9 are presented as graphics in Figure 6.7.

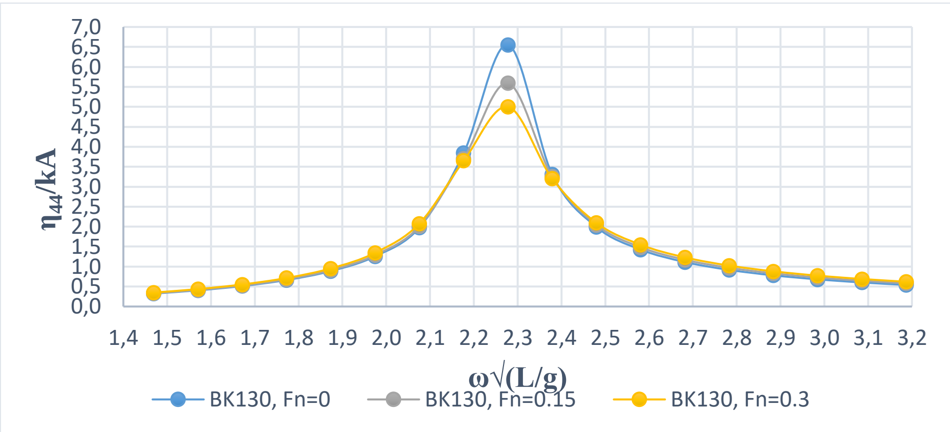

Figure 6.7 : BK130 bilge keel non-dimensional roll η_{44}/kA graphics.

Table 6.10 presents the η_{44}/kA values of DTMB 5415 model mounted BK230 bilge keel model.

Table 6.10 : BK230 bilge keel non-dimensional roll η_{44}/kA values.

BK230, Fn=0			BK230, Fn=0,15			BK230, Fn=0,30		
ω (rad/s)	$\omega\sqrt{\frac{L}{g}}$	η_{44}/kA	ω (rad/s)	$\omega\sqrt{\frac{L}{g}}$	η_{44}/kA	ω (rad/s)	$\omega\sqrt{\frac{L}{g}}$	η_{44}/kA
2.580	1.427	0.296	2.580	1.427	0.305	2.580	1.427	0.322
2.757	1.524	0.367	2.757	1.524	0.378	2.757	1.524	0.399
2.934	1.622	0.459	2.934	1.622	0.472	2.934	1.622	0.499
3.111	1.720	0.582	3.111	1.720	0.599	3.111	1.720	0.633
3.288	1.818	0.756	3.288	1.818	0.779	3.288	1.818	0.824
3.465	1.916	1.021	3.465	1.916	1.053	3.465	1.916	1.114
3.642	2.014	1.472	3.642	2.014	1.517	3.642	2.014	1.604
3.819	2.112	2.400	3.819	2.112	2.456	3.819	2.112	2.574
3.997	2.210	4.963	3.997	2.210	4.801	3.997	2.210	4.763
4.174	2.308	6.231	4.174	2.308	5.755	4.174	2.308	5.421
4.351	2.406	3.099	4.351	2.406	3.149	4.351	2.406	3.208
4.528	2.504	1.964	4.528	2.504	2.049	4.528	2.504	2.145
4.705	2.602	1.443	4.705	2.602	1.523	4.705	2.602	1.614
4.882	2.700	1.146	4.882	2.700	1.219	4.882	2.700	1.301
5.059	2.798	0.953	5.059	2.798	1.021	5.059	2.798	1.094
5.236	2.896	0.817	5.236	2.896	0.879	5.236	2.896	0.945
5.414	2.994	0.715	5.414	2.994	0.773	5.414	2.994	0.833
5.591	3.092	0.636	5.591	3.092	0.689	5.591	3.092	0.744

The values in Table 6.10 are presented as graphics in Figure 6.8.

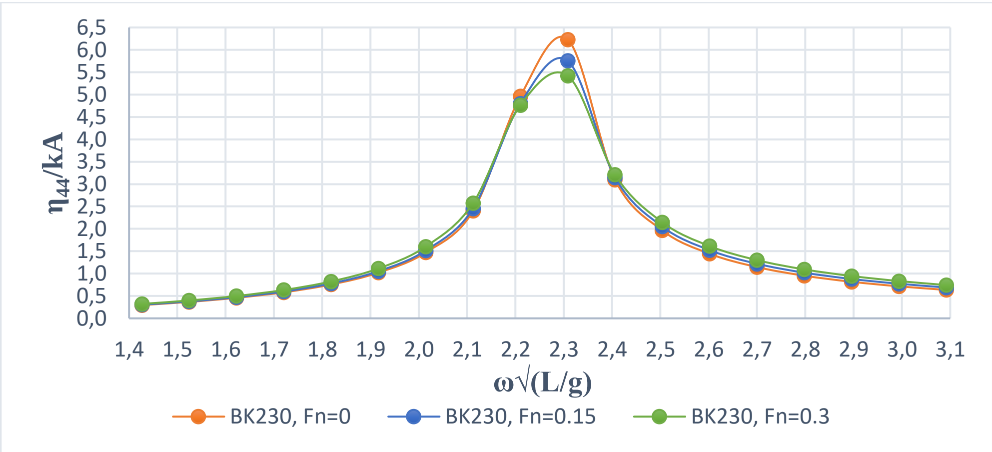

Figure 6.8 : BK230 bilge keel non-dimensional roll η_{44}/kA graphics.

According to tables and graphics shown above, η_{44}/kA values at natural frequencies for variable Froude numbers presented in Table 6.11.

Table 6.11 : Non-dimensional roll η_{44}/kA values at natural frequencies.

Fn	BK060	BK160	BK260	BK030	BK130	BK230
0	6.593	6.734	6.195	7.047	6.554	6.231
0.15	6.093	5.999	5.777	6.395	5.592	5.755
0.30	5.761	5.530	5.483	5.981	5.000	5.421

By Table 6.11, it can be said that for Fn=0 the best bilge keel option for roll damping is BK260. However, the situation changes for Fn=0.15 which the best bilge keel option is BK130. For Fn=0.3 again the best option for bilge keel choice is BK130.

Table 6.12 : Non-dimensional roll η_{44}/kA damping (%) at natural frequencies.

Fn	BK060	BK160	BK260	BK030	BK130	BK230
0-0.15	8.196	12.247	7.227	10.201	17.192	8.262
0.15-0.3	5.762	8.479	5.360	6.928	11.839	6.172

In Table 6.12, roll damping percentage for each bilge keel model for Froude number 0 to 0.15 and 0.15 to 0.30 observed. According to Table 6.12 it can be observed that BK130 bilge keel model damping percentage is higher than other bilge keel options.

7. CONCLUSIONS

Linear seakeeping theory is highly effective for predicting the seakeeping behavior of conventional vessels, offering both high accuracy and quick results. However, for the design of unconventional ships, offshore structures, or for predicting the motions of vessels in extreme weather conditions, the 3D panel method may be preferred.

In this study, the validation of experimental result was performed for DTMB 5415 ship bare hull by using 3-D panel method based software AQWA©. These studies were conducted for roll motion to evaluate RAO values. The comparison for AQWA© and experimental results were promising. Subsequently, to observe the impact of various bilge keels to roll motion of 5415 vessel, six different type of bilge keels are modelled and studied.

BK060 was the initial bilge keel simulated, representing the original design for the 5415 hull. In comparison to the bare hull, BK060 achieves an 11% reduction in roll RAO at a forward speed Fn=0.

The second bilge keel, BK160, is projected to decrease roll motion RAO by approximately 8.71%. BK260 demonstrates a more significant reduction, with an estimated mitigation of 18.17% in roll motion. In contrast, BK030 provides a reduction of about 3.88%, while BK130 yields an approximate 11,7% decrease in roll motion, and BK230 results in a 17.49% reduction when compared to the bare hull model of the DTMB 5415.

For the Fn = 0 scenario, it is evident that BK260 and BK230 exhibit superior performance relative to the other bilge keels. However, it is important to analyze the impact of forward speed on bilge keel efficiency. Therefore, performance assessments were conducted for Fn values ranging from 0 to 0.15 and from 0.15 to 0,30.

As shown in Table 5.9, BK260 and BK230 are no longer the optimal choices under forward speed conditions. Instead, BK130 emerges as the best option, achieving a roll motion reduction of approximately 17.19% for Fn = 0 to 0.15, and 11.839% for Fn =

0.15 to 0.30. The second most effective bilge keel, according to Table 5.9, is BK160, which results in a roll motion decrease of approximately 12.247% for Fn = 0 to 0.15 and 8.479% for Fn = 0.15 to 0.30.

Based on these computations the following guidelines are reccommended regarding the angle and dimensions of bilge keels for high speed displacement type vessels:

a) The angle of the bilge keel should be 30 degrees,
b) The length of the bilge keel should be 59 meters,
c) The width of the bilge keel should be 0.7 meters.

The recommendations provided above are intended for the full-scale DTMB 5415 high-speed displacement type vessel. Modifications to the suggestions may be necessary for vessels of the same type but different form.

Several studies have investigated the influence of bilge keel width on the mitigation of roll motion. This thesis indicates that the width, length, and angle of the bilge keels, as well as the vessel's forward speed, must be considered simultaneously to make an informed decision regarding the selection of the most appropriate bilge keel for a specific hull design.

REFERENCES

[1] **Froude, W.** (1861.)On the rolling of ships. Institution of Naval Architects.

[2] **Keulegan, G. and Carpenter, L.** (1958). Forces on cylinders and plates in an oscillating fluid. Journal of Research of the National Bureau of Standards, 60(5), 423.

[3] **Vugts, J.** (1968). The hydrodynamic coefficients for swaying, heaving and rolling cylinders in a free surface1. International Shipbuilding Progress, 15(167), 251–276.

[4] **Ikeda, Y.** (1976). Ship roll damping - frictional component and normal pressure on bilge keel. Journal of The Kansai Society of Naval Architects, vol. 161,

[5] **Brown, D. T. and Patel, M. H.** (1985). A theory for vortex shedding from the keels of marine vehicles. Journal of Engineering Mathematics, 19(4), 265–295.

[6] **Sarpkaya, T. and O'Keefe, J. L.** (1996). Oscillating Flow About Two and Three-Dimensional Bilge Keels. Journal of Offshore Mechanics and Arctic Engineering, 118(1), 1–6.

[7] **Chakrabarti, S. K.** (2001). Empirical calculation of roll damping for ships and barges. Ocean Engineering, 28(7), 915–932.

[8] **Taylan, M.** (2004). Effect of Forward Speed on Ship Rolling and Stability. Mathematical and Computational Applications, 9(2), 133–145.

[9] **Zaraphonitis, G. and Papanikolaou,** A. (2004). On the numerical prediction of seakeeping and of structural loads of high-speed vessels. Applied Ocean Research, 26(6), 274–287.

[10] **Ikeda, Y.** (2005). Prediction methods for parametric rolling under drifting condition and their validation.6th Osaka colloquium on seakeeping and stability of ships.

[11] **Bassler, C.C.** (2009). An Analysis of The Bilge Keel Roll Damping Component Model. 10th International Conference on Stability of Ships and Ocean Vehicles.

[12] **Graham, J. M. R.** (2011). The application of lagrangian vortex methods to the prediction of hydrodynamic damping of floating bodies. II International Conference on Particlebased Methods - Fundamentals and Applications, 184–192.

[13] **Jaouen, F., Koop, A., Vaz, G., and Crepier, P.** (2011). Rans predictions of roll viscous damping of ship hull sections. International Conference on Computational Methods in Marine Engineering, 76–93.

[14] **Miyake, T.** (2013). A study on roll damping of bilge keels for new non-ballast ship with rounder cross section. Proceedings of the 13th International Ship Stability Workshop.

[15] **Irkal, M., Nallayarasu, S. and Bhattacharyya, S.K.** (2014). Experimental And CFD Simulation of Roll Motion of Ship With Bilge Keel International Conference on Computational and Experimental Marine Hydrodynamics , Chennai.

[16] **Deng, R., Duan, W., Ma, S., and Ma, Y.** (2015). Numerical Research of the Viscous Effect of the Bilge Keel on the Damping Moment. Polish Maritime Research, 22(s1), 67–74.

[17] **Counsil, J., McTaggart, K., Groulx, D., and Boulama, K.** (2015). Ship Roll Motion Damping Using Bilge Keels – A Detailed CFD Investigation. Minister of National Defence.

[18] **Falzarano, J., Somayajula, A., and Seah, R.** (2015). An overview of the prediction methods for roll damping of ships. Ocean Systems Engineering, 5(2), 55–76.

[19] **Gu, Y., Boulougouris, E., and Day, A.** (2015). A study on the effects of bilge keels on roll damping coefficient. 12th International Conference on the Stability of Ships and Ocean Vehicles.

[20] **Haver, T.** (2016). Roll Damping Prediction for Vessels; Sheerlegs and Barges: A study on effects of viscosity and roll-sway coupling on the roll damping coefficient. MSc Thesis.

[21] **Park, D., Lee, J., and Kim, Y.** (2015). Uncertainty analysis for added resistance experiment of KVLCC2 ship. Ocean Engineering, 95, 143–156.

[22] **Yıldız, B., Çakıcı, F., Katayama, T. and Yılmaz, H.** (2015). URANS prediction of roll damping for a ship hull section at shallow draft. Journal of Marine Science and Technology, 21(1), 48–56.

[23] **Ommani, B., Fonseca, N., Kristiansen, T., Hutchison, C., and Bakksjø, H.** (2016). Bilge Keel Induced Roll Damping of an FPSO With Sponsons. Proceedings of the ASME 2016 35th International Conference on Ocean, Offshore and Arctic Engineering.

[24] **Irkal, M. A., Nallayarasu, S., and Bhattacharyya, S.** (2016). CFD approach to roll damping of ship with bilge keel with experimental validation. Applied Ocean Research, 55, 1–17.

[25**] Jiang, Y.** (2017). Bilge-Keel Influence on Free Decay of Roll Motion of a Realistic Hull. Journal of Offshore Mechanics and Arctic Engineering, no. 139, 2017.

[26] **Gokce, M. K., and Kinaci, O. K.** (2018). Numerical simulations of free roll decay of DTMB 5415. Ocean Engineering, 159, 539–551.

[27] **Irkal, M. R., Nallayarasu, S., and Bhattacharyya, S. K.** (2016b). CFD Simulation of Roll Damping Characteristics of a Ship Mid-Section With Bilge Keel. Proceedings of the ASME 2016 35th International Conference on Ocean, Busan.

[28] **Yildiz, B., and Yilmaz, H**. (2017). Numerical Investigation of the Effect of Bilge Keel Width on Roll Damping. Gemi Ve Deniz Teknolojisi, 22(209), 31–43.

[29] **Irkal, M. A., Nallayarasu, S., and Bhattacharyya, S. K.** (2016). CFD Simulation of Roll Damping Characteristics of a Ship Mid-Section With Bilge Keel. Proceedings of the ASME 2016 35th International Conference on Ocean.

[30] **Kim, M., Jung, K., Park, S., Suh, S., Park, I., Kim, J., and Kim, K.** (2019). Experimental study on viscous effect in roll and heave motions of a rectangular structure. Ocean Engineering, 171, 250–258.

[31] **Lungu, A.** (2020). A Numerical Study of the Roll Damping for Double-Symmetric Bodies. Procedia Manufacturing, 46, 475–483.

[32] **Ibinabo, I., and Tamunodukobipi, D. T.** (2019). Determination of the Response Amplitude Operator(s) of an FPSO. Engineering, 11(09), 541–556.

[33] **Asis, M. A., Paroka, D., Asri, S., and Syam, M. A.** (2020). Effect of Bilge Keels Position On Roll Motion Performance Of Traditional Wooden Boat. International Journal of Marine Engineering Innovation and Research, 5(3).

[34] **Jiang, Y., Ding, Y., Sun, Y., Shao, Y., and Sun, L.** (2020). Influence of bilge-keel configuration on ship roll damping and roll response in waves. Ocean Engineering, 216, 107539.

[35] **Walree, F.** (2020). Prediction of Heavy Weather Seakeeping of a Destroyer Hull Form by Means of Time Domain Panel and CFD Codes. 33rd Symposium on Naval Hydrodynamics, Osaka.

[36] **Deng, R., Chen, S., Luo, F., Wang, Y., and Wu, T.** (2021). Numerical study on viscous flow field of forced rolling of ships with bilge keels. Ocean Engineering, 239.

[37] **Alexandersson, M., Kjellberg, M., Mao, W. And Ringsberg, J.** (2021). Prediction of Roll Motion Using Fully Nonlinear Potential Flow and Ikeda's Method.

[38] **Molland, A.** (2008). A Guide to Ship Design, Construction and Operation. The Maritime Engineering Reference Book, Butterworth Heinemann,p. 490.

[39] **Barr, R. A., and Ankudinov, V.** (1977). Ship Rolling, Its Prediction and Reduction Using Roll Stabilization. Marine Technology and SNAME News, 14(01), 19–41.

[40] **Miller, E. R., Slager, J. J., and Webster, W. C.** (1974). Development of a Technical Practice for Roll Stabilization System Selection. Phase I. NAVSEC, Maryland.

[41] **Baniela,S.** (2008). Roll Motion of a Ship and the Roll Stabilising Effect of Bilge Keels. The Journal of Navigation, no. 61, 2008.

[42] **Ikeda, Y.** (2004). Prediction Methods of Roll Damping of Ships and Their Application to Determine Optimum Stabilization Devices. Marine Technology and SNAME News, 41(02), 89–93.

[43] **Wilson, R. V., Carrica, P. M., and Stern, F.** (2006). Unsteady RANS method for ship motions with application to roll for a surface combatant. Computers and Fluids, 35(5), 501–524.

[44] **Bangun, E., Wang, C., and Utsunomiya, T.** (2010). Hydrodynamic forces on a rolling barge with bilge keels. Applied Ocean Research, 32(2), 219–232.

[45] **Van 't Veer, R., Fathi, F., and Kherian, J. G.** (2011). On Roll Hydrodynamics of FPSO's Fitted With Bilge Keels and Riser Balcony. 30th International Conference on Ocean,Offshore and Arctic Engineering. pp. 257-268

[46] **Thiagarajan, K. P., and Braddock, E. C.** (2009). Influence of Bilge Keel Width on the Roll Damping of FPSO. Journal of Offshore Mechanics and Arctic Engineering, 132(1).

[47] **Avalos, G. O., Wanderley, J. B., Fernandes, A. C., and Oliveira, A. C.** (2014). Roll damping decay of a FPSO with bilge keel. Ocean Engineering, 87, 111–120.

[48] **Ikeda, Y., Ali, B., and Yoshida, H.** (2004). A Roll Damping Prediction Method For a FPSO With Steady Drift Motion. The Fourteenth International Offshore and Polar Engineering Conference.

[49] **Rahmaji, T., Prabowo, A. R., Muhayat, N., Tuswan, T., and Putranto, T.** (2023). Effect of bilge keel variations on the designed fast patrol boats to hull resistance and stability behaviours. IOP Conference Series Earth and Environmental Science, 1166(1).

[50] **Van Daalen, E., Kleefsman, K., Gerrits, J., Luth, H., and Veldman, A.** (2001). Anti-Roll Tank Simulations with a Volume of Fluid (VOF) Based Navier-Stokes Solver. Twenty-Third Symposium on Naval Hydrodynamics, Washington, DC.

[51] **Youssef, K. S., Ragab, S. A., Nayfeh, A. H., and Mook, D. T.** (2002). Design of passive anti-roll tanks for roll stabilization in the nonlinear range. Ocean Engineering, 29(2), 177–192.

[52] **Ziegler, P.E.** (1966). Anti Roll Tank Design, Massachusetts.

[53] **Novac, I., and Faitar, C.** (2016). Consideration Upon Fixed Anti - Rolling Passive Systems. Scientific Bulletin of Naval Academy, 19(2).

[54] **Cinal, Ş., Eminoğlu, İ.** (2022). Mechanical Gyroscope-Based Roll Motion Reduction of Marine Vehicles: An Educational Setup. Journal of Naval Sciences and Engineering , no. 18, pp. 179-204.

[55] **Demir, U.** (2020). Use of Anti Rolling Gyro (ARG) Optimization Systems For Planing Boats. Uluslararası Doğu Anadolu Fen Mühendislik ve Tasarım Dergisi , no. 2, pp. 247-261.

[56] **Alaswad, K.** (2020). Gyro Moment Stabilizer For 10m Yachts. M.Sc. Thesis.

[57] **Halse, K., , V. and Sporsheim, O.** (2012). An Active Roll Reduction System Using Free Flooding Tanks Controlled By Vacuum Pumps.

[58] **Lew, J., Kim, H., and Choi, B.** (2002). Development of Passive And Active Anti-Rolling Tanks. The Fifth ISOPE Pacific/Asia Offshore Mechanics Symposium, Daejeon.

[59] **Moaleji, R., and Greig, A. R.** (2007). On the development of ship anti-roll tanks. Ocean Engineering, 34(1), 103–121.

[60] **Marzouk, O. A., and Nayfeh, A. H.** (2009). Control of ship roll using passive and active anti-roll tanks. Ocean Engineering, 36(9–10), 661–671.

[61] **Gunsing,M., Carette, N. and Kapsenberg, G.** (2014). Experıiental Data On The Systematic Variation Of The Internal Damping Inside A U-Shaped Anti-Roll Tank. Proceedings of the ASME 2014 33rd International Conference on Ocean, Offshore and Arctic Engineering , San Francisco.

[62] **Alujević, N., Ćatipović, I., Malenica, Š., Senjanović, I., and Vladimir, N.** (2020). Stability, performance and power flow of active U-tube anti-roll tank. Engineering Structures, 211.

[63] **Sen, D., Saripilli, J.** (2012). A Study On The Effectiveness Of Active Fin RollStabilizers Through Numerical Simulation. International Journal of Innovative Research and Development, no. 1.

[64] **Kula, K. S.** (2015). An Overview of Roll Stabilizers and Systems for Their Control. TransNav the International Journal on Marine Navigation and Safety of Sea Transportation, 9(3), 405–414.

[65] **Patil, N. S., Dubey, A. C., and Subramanian, V. A.** (2019). Fin based active control for ship roll motion stabilization. MATEC Web of Conferences, 272.

[66] **Lloyd, A. R. J. M.** (1998). Seakeeping: Ship Behaviour in Rough Weather.

[67] **Gatzoulis, J., and Keane, R. G.** (1977). Upgrading Mission Capability And Performance Effectiveness Of Naval Ships By The Use Of Actıve Fın Stabilizers. 14th Annual Technical Symposium , Washington,.

[68] **Fan, W., Hongzhang, J., and Zhigang, Q.** (2009). Modeling for active fin stabilizers at zero speed. Ocean Engineering, 36(17–18), 1425–1437.

[69] **Tzeng, C., Wu, C., and Chu, Y.** (2001). A Sensitivity Function Approach to the Design of Rudder Roll Stabilization Controller. Journal of Marine Science and Technology, 9(2).

[70] **Baitis, A. E.** (1980). The Development And Evaluation Of A Rudder Roll Stabilizatıon System For The WHEC Hamilton Class. Bethsada.

[71] **Santoso, M. Y., Munadhif, I., Wahidin, A., Ruddianto, N., Fathulloh, N., and Soelistijono, R. T.** (2017). Rudder-roll stabilization using fgs-pid controller for sigma-e warship. Journal of Physics Conference Series, 855.

[72] **Sgobbo, J. N., and Parsons, M. G.** (1999). Rudder/Fin Roll Stabilization of the USCG WMEC 901 Class Vessel. Marine Technology and SNAME News, 36(03), 157–170.

[73] **Zihnioğlu, A., and Ünsan, Y.** (2016). Gemiler İçin Yalpa Sönümleyici Sistemler. GİDB Dergi, 07, 3–14.

[74] **STANAG4154**, Common Procedures for Seakeeping in the Ship Design Process Annex-A A-14.

[75] **Hsueh, W., and Lee, Y.** (1997). A design for ship stabilization by activated antiroll tanks. Journal of Marine Science and Technology, 2(2), 77–86.

[76] **ANSYS.** (2015). AQWA Theory Manual, pp. 27-77

[77] **Ursell, F.** (1954). Water Waves Generated by Oscillating Bodies, Journal of Mechanics and Applied Mathematics, no. 7, pp. 427-437.

[78] **Frank, W., and Salvesen, N.** (1970). The Frank Close-Fit Ship-Motion Computer Program. Washington DC.

[79] **Ikeda, Y.** (2011). Numerical Estimation of Roll Damping. International Towing Tank Conference-Recommended Procedures and Guidelines.

[80] **Ikeda, Y., Himeno, Y., and Tanaka, N.** (1978). Components of Roll Damping of Ship at Forward Speed. Journal of the Society of Naval Architects of Japan, 1978(143), 113–125.

[81] **ANSYS.** (2015). AQWA Theory Manual. pp. 157-159

[82] **Bailardi, G.** (2014). Seakeping Analysis of Sailing Yacht Hulls and Centerboard Effect: Comparison Between Potential Method and CFD RANS. Master Thesis. Genoa.

[83] **Mancini, S.** (2018). Verification and Validation of Numerical Modelling of DTMB 5415 Roll Decay. Ocean Engineering, no. 162, pp. 209-233.

[84] **Begovic, E.** (2013). Experimental Assesment of Intact and Damaged Ship Motions in Head, Beam and Quartering Seas. Ocean Engineering, no. 72, pp. 209-226.

[85] **US Navy Combatant,** DTMB 5415, SIMMAN 2008, FORCE Technology. (n.d.). http://www.simman2008.dk/5415/combatant.htm

[86] **Lewandowski, E.** (2004). The Dynamics of Marine Craft Maneuvering and Seakeeping, pp. 265-277

CIRRUCULUM VITAE

Name Surname	**:**	Erhan SÖKMEN

EDUCATION

B.Sc.	**:**	2018, Trakya University, Engineering Faculty, Mechanical Engineering Department